

## 8. SITE 932<sup>1</sup>

### Shipboard Scientific Party<sup>2</sup>

#### HOLE 932A

**Date occupied:** 11 April 1994  
**Date departed:** 12 April 1994  
**Time on hole:** 1 day, 3 hr  
**Position:** 5°12.682'N, 47°1.770'W  
**Bottom felt (drill pipe measurement from rig floor, m):** 3344.5  
**Distance between rig floor and sea level (m):** 10.90  
**Water depth (drill pipe measurement from sea level, m):** 3333.6  
**Penetration (m):** 168.30  
**Number of cores (including cores having no recovery):** 18  
**Total length of cored section (m):** 168.30  
**Total core recovered (m):** 154.71  
**Core recovery (%):** 91  
**Oldest sediment cored:**  
Depth (mbsf): 168.30  
Nature: Silty clay  
Earliest age: Pleistocene

#### HOLE 932B

**Date occupied:** 12 April 1994  
**Date departed:** 12 April 1994  
**Time on hole:** 12 hr, 15 min  
**Position:** 5°12.690'N, 47°1.770'W  
**Bottom felt (drill pipe measurement from rig floor, m):** 3347.0  
**Distance between rig floor and sea level (m):** 10.90  
**Water depth (drill pipe measurement from sea level, m):** 3336.1  
**Penetration (m):** 52.50  
**Number of cores (including cores having no recovery):** 6  
**Total length of cored section (m):** 52.50  
**Total core recovered (m):** 54.09  
**Core recovery (%):** 103  
**Oldest sediment cored:**  
Depth (mbsf): 52.50  
Nature: Silty clay  
Earliest age: Pleistocene  
**Principal results:** Site 932 (proposed Site AF-11) is located on the eastern part of the Amazon Fan, 200 m east of the crest of the western levee of

abandoned Channel-levee System 6B. The site was intended to provide a hemipelagic biostratigraphic and magnetostratigraphic reference section above Channel-levee System 6B and to sample the upper part of the levee crest. This channel-levee system is the stratigraphically oldest part of the Upper Levee Complex, and, based on the results at Site 930, we thought it possible that we would reach sediment from late in the last interglacial.

The site was selected from a *Ewing* seismic-reflection profile (E9209; 0635UTC on 21 Sept.). High-resolution seismic-reflection data through the planned drilling interval were obtained from the pre-site survey from *JOIDES Resolution*.

Hole 932A was cored by advanced piston corer (APC) to 91.5 mbsf, then by extended core barrel (XCB) to 168.3 mbsf, with total hole recovery of 154.71 m (91.9%). Hole 932B was cored to 52.5 mbsf and recovered 54.09 m (103.0%).

Temperature measurements at 63 and 82 mbsf (ADARA) and at 120 mbsf (WSTP) yielded a mean geothermal gradient of 31°C/km, with a higher gradient in the upper part of the hole. There was gas expansion in many cores. Methane was found throughout the hole, but higher hydrocarbons were not detected.

Two lithologic units are recognized:

Unit I (0–0.70 mbsf) is a Holocene nannofossil-foraminifer clay, bioturbated, with about 50% carbonate.

Unit II (0.70–168.30 mbsf) consists of mud with interbedded laminae and beds of silt and very fine sand. The mud has about 3% carbonate content. The unit is subdivided into two subunits, analogous to those at Sites 930 and 931. Subunit IIA (0.63–47.0 mbsf) comprises bioturbated mud. Disturbed sediment (probably a debris-flow deposit) is found at 41–42 mbsf. This subunit represents sediment that accumulated since the abandonment of Channel 6B. Subunit IIB (47.0 to 168.3 mbsf) contains the youngest sediment from the crest of the Channel 6B levee. This subunit is composed of mud with thin to thick beds of silt and fine sand, which increase in frequency and thickness toward the base of the subunit, particularly below 130 mbsf.

Foraminifer abundances are generally moderate in Subunit IIA and low in Subunit IIB. At 44 mbsf, abundant *P. obliquiloculata* reappears, suggesting an age >40 ka. The Lake Mungo magnetic excursion (30 ka), was found at 24 mbsf. Variation in magnetic declination, interpreted as secular variation, was detected with nine cycles between 31 and 43 mbsf.

A palynological study was made of three stratigraphic levels: Holocene, last glacial (20 ka), and the *P. obliquiloculata* datum (40 ka). The Holocene section is nearly barren. Last glacial assemblages are well preserved and diverse. The major pollen types include Euphorbiaceae, Rhizophoraceae, Gramineae, Cyperaceae, tricolporate, tricolpate, and stephanoporate types. Fern spores include Cyatheaceae, Lycopodiidae, and monolete spores. The pollen and spore assemblage from the 40-ka level contains lower abundances and diversities than the last glacial assemblage. Major pollen types include tricolporate and tricolpate types and Cyperaceae. Fern spores include Cyatheaceae, trilete, and monolete spores.

Pore-water data, the abundance of methane, and total organic carbon contents were similar to those observed at Sites 930 and 931. In general, physical properties data also show trends similar to those established at Sites 930 and 931. Unusually low bulk density and high water content between 14 and 21 mbsf may relate to increased sedimentation rate, diagenetic hydrotroilite formation, or the presence of trapped gas beneath a

<sup>1</sup>Flood, R.D., Piper, D.J.W., Klaus, A., et al., 1995. *Proc. ODP, Init. Repts.*, 155: College Station, TX (Ocean Drilling Program).

<sup>2</sup>Shipboard Scientific Party is as given in the list of participants in the contents.

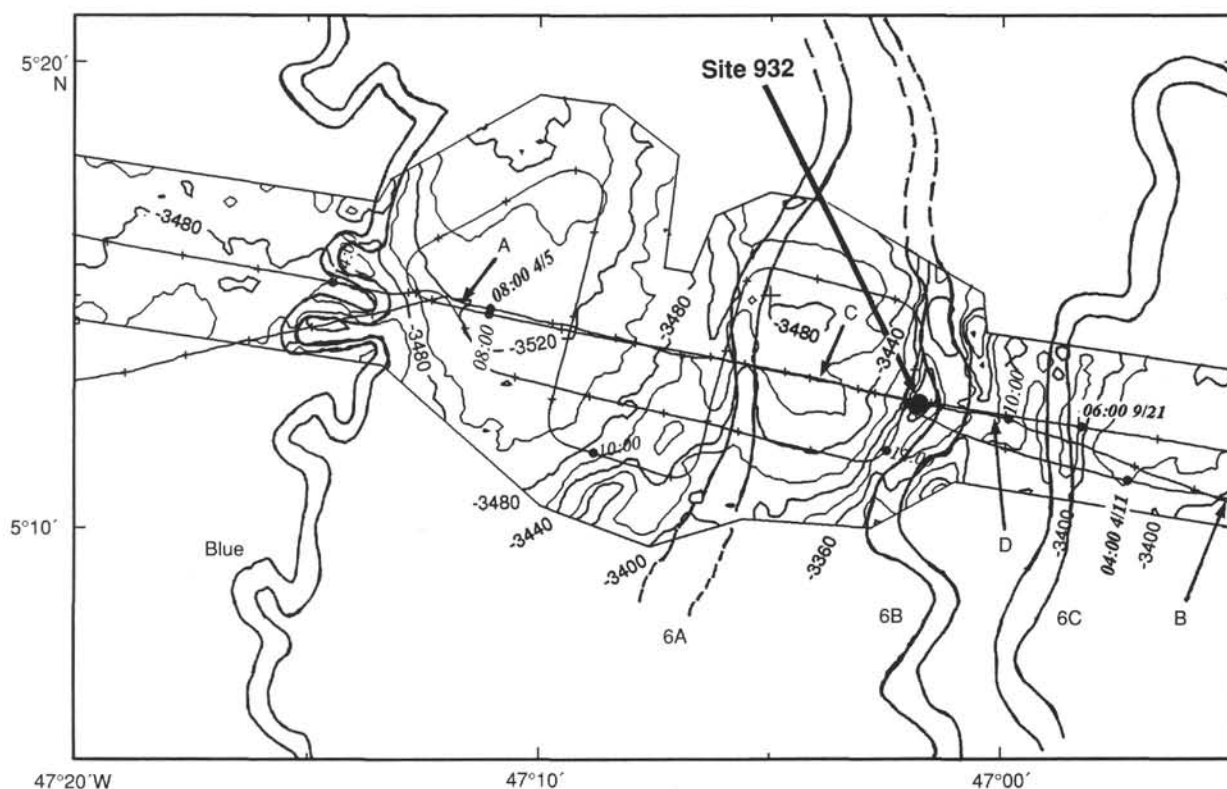


Figure 1. Location of Site 932 showing *JOIDES Resolution* tracks. A–B is seismic profile in Figure 3. C–D is 3.5-kHz profile in Figure 2. Bathymetry from Flood et al. (1991) and from *Ewing* cruise 9209. Channels are based on *GLORIA* long-range sidescan images (Damuth et al., 1988).

clathrate horizon. No clathrate were observed in the cores, although gas expansion occurred in cores retrieved from this interval.

The shipboard data from Site 932 confirm the biostratigraphic and magnetostratigraphic markers established at Site 930. The sequence of bioturbated muds with rare silt laminae above Channel-levee System 6B is about 46 m thick, and the upper 45 m of the levee is also considerably bioturbated, suggesting relatively low sedimentation rates. The levee section that was cored is a fining-upward sequence of turbidites. Extrapolating sedimentation rates from the upper 45 mbsf suggests that Channel-levee System 6B dates from about 60–80 ka, immediately following the last interglacial.

## SETTING AND OBJECTIVES

### Introduction

Site 932 (proposed Site AF-11) was intended to provide a partially hemipelagic reference section above the levee of Channel 6B and to sample the upper part of the Channel 6B levee crest. Channel 6 represents the deepest part of the Upper Levee Complex (Manley and Flood, 1988) and, based on the results at Site 930, we hoped to reach sediment deposited late in the last interglacial (oxygen isotopic Stage 5a).

### Setting

Site 932 is located on the eastern part of the Amazon Fan, on a flat terrace 200 m east of the crest of the western (left) levee of Channel 6B and about 700 m from the channel margin (Figs. 1 and 2). The age of Channel 6 is uncertain from seismic profiles, but it appears to immediately pre-date the Orange Channel-levee System in the central part of the fan (Table 1 of "Introduction" chapter, this volume). It is probably the oldest channel-levee system of the Upper Levee Complex.

The site was selected from a *Ewing* seismic profile (E9209; 0635UTC on 21 Sept.). High-resolution seismic data through the planned drilling interval were obtained from the pre-site survey from *JOIDES Resolution* (Fig. 3).

The surficial sediment at the site, interpreted from 3.5-kHz sub-bottom profiles, shows a surface drape of acoustically stratified sediment about 16 ms thick overlying a more transparent section 8 ms thick (Fig. 2). The upper unit maintains its thickness across the levee flank, but the lower unit thins to 6 ms over a distance of 4 km westward away from the channel. The thickness of hemipelagic sediment above the crest of the Channel 6B levee cannot be determined from seismic profiles. The HARP at the base of the levee is at about 275 mbsf and was not a target at this site.

### Objectives

The principal objectives at Site 932 were:

1. To sample the anticipated hemipelagic section above the Channel 6 levee to extend the biostratigraphic and paleomagnetic record back farther in time than was achieved at Site 930.
2. To sample the sediment of the levee crest of Channel 6B, for a record of detritus from the continent.

## OPERATIONS

### Seismic Survey: Site 931 to Site 932 (AF-11)

Based on results at Site 931, additional seismic information was needed to adjust Site 933 (AF-9) that would be drilled after Site 932 (AF-11). We, therefore, conducted a seismic survey (about 43 nmi) along the crest of the deep, buried levee in the vicinity of AF-9. We then moved to Site 932.

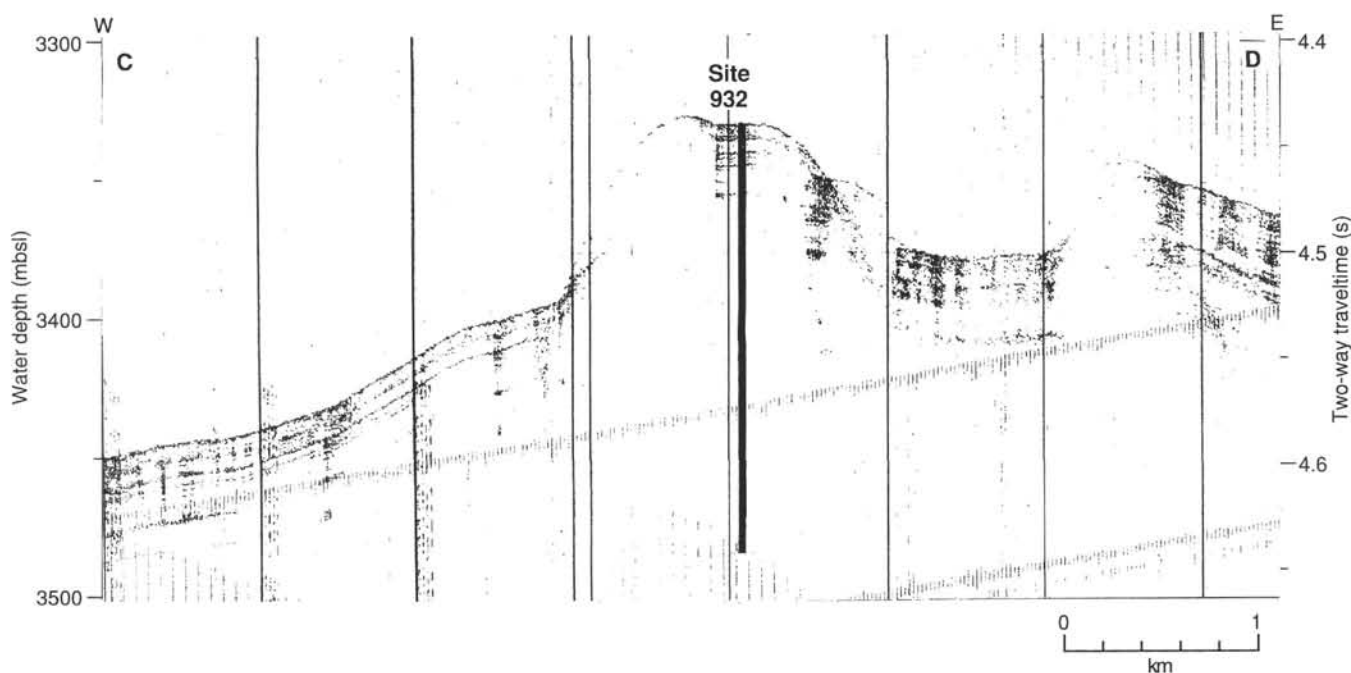


Figure 2. A 3.5-kHz profile through Site 932. (JOIDES Resolution, 0920–0957UTC on 5 April 1994).

Table 1. Site 932 coring summary.

Core	Date (1994)	Time (UTC)	Depth (mbsf)	Length cored (m)	Length recovered (m)	Recovery (%)
<b>155-932A-</b>						
1H	April 11	1200	0.0–6.0	6.0	6.00	100.0
2H	April 11	1255	6.0–15.5	9.5	9.62	101.0
3H	April 11	1405	15.5–25.0	9.5	10.50	110.5
4H	April 11	1505	25.0–34.5	9.5	10.15	106.8
5H	April 11	1555	34.5–44.0	9.5	10.43	109.8
6H	April 11	1640	44.0–53.5	9.5	10.29	108.3
7H	April 11	1755	53.5–63.0	9.5	10.37	109.1
8H	April 11	1920	63.0–72.5	9.5	6.47	68.1
9H	April 11	2030	72.5–82.0	9.5	10.14	106.7
10H	April 11	2120	82.0–91.5	9.5	9.75	102.0
11X	April 11	2235	91.5–101.0	9.5	7.27	76.5
12X	April 11	2335	101.0–110.6	9.6	9.43	98.2
13X	April 12	0030	110.6–120.3	9.7	7.03	72.5
14X	April 12	0240	120.3–130.0	9.7	7.56	77.9
15X	April 12	0355	130.0–139.7	9.7	7.75	79.9
16X	April 12	0455	139.7–149.2	9.5	6.09	64.1
17X	April 12	0605	149.2–158.7	9.5	7.13	75.0
18X	April 12	0720	158.7–168.3	9.6	8.73	90.9
Coring totals				168.3	154.7	91.90
<b>155-932B-</b>						
1H	April 12	0935	0.0–5.0	5.0	5.05	101.0
2H	April 12	1020	5.0–14.5	9.5	8.46	89.0
3H	April 12	1115	14.5–24.0	9.5	9.89	104.0
4H	April 12	1210	24.0–33.5	9.5	9.93	104.0
5H	April 12	1300	33.5–43.0	9.5	10.45	110.0
6H	April 12	1345	43.0–52.5	9.5	10.31	108.5
Coring totals				52.5	54.1	103.00

Note: An expanded version of this coring summary table that includes lengths and depths of sections, location of whole-round samples, and comments on sampling disturbance is included on the CD-ROM in the back pocket of this volume.

### Hole 932A

After retrieving the seismic gear, we returned to the GPS coordinates 05°12.683'N, 47°01.770'W and deployed a beacon at 0131 hr 11 April. We assembled a bottom-hole assembly (BHA) similar to that used at Sites 930 and 931 and ran the bit to the seafloor. Depend-

ing on the ship's draft, the distance from sea level to rig floor was 10.90 m for Holes 932A and 932B. The 3.5-kHz depth recorded indicated a depth of 3382.4 mbrf.

We positioned the bit at 3341.0 mbrf and spudded Hole 932A at 0742 hr 11 April. Core 1H recovered 6.00 m of sediment (Table 1). The mud line was defined to be 3344.5 mbrf. Cores 1H through 10H were taken from 3344.5 to 3436.0 mbrf (0–91.5 mbsf) recovering 93.21 m of sediment (102% recovery). In most of the cores recovered at Site 932, sediment began to extrude from the core liner due to gas expansion once the liner was taken out of the core barrel. Core disturbance was minimized by drilling small holes in nearly all of the core liners to allow gas to escape.

Cores 3H through 10H were oriented using the Tensor tool, and ADARA heat-flow measurements were made during Cores 7H and 9H. During APC coring, core liners ruptured occasionally, in some cases significantly disturbing the recovered sediment.

XCB Cores 11X through 18X were taken from 3436.0 to 3512.8 mbrf (91.5–168.3 mbsf), coring 76.8 m and recovering 61.06 m (80%). The WSTP tool was run prior to Core 14X. The combined APC/XCB recovery was 91.6%. The hole angle was 1.6° at 25.0 mbsf, 2.7° at 34.5 mbsf, 2.5° at 63.0 mbsf, and 3.0° at 82.0 mbsf. We pulled the bit above the seafloor at 0430 hr 12 April.

### Hole 932B

We moved the ship 20 m north and spudded Hole 932B at 0513 hr 12 April. The bit was positioned at 3342.5 mbrf, and Core 1H recovered 5.05 mbrf. The seafloor was defined to be at 3347.0 mbrf. We attempted to offset Core 1H from Hole 932A in an effort to recover a possible magnetic event and should have recovered 7.5 m. We took Cores 1H through 6H from 3347.0 to 3399.5 mbrf (0–52.5 mbsf) and recovered 54.04 m of sediment (103% recovery). Cores 3H through 6H were oriented using the Tensor tool. The hole angle was 1.9° at 24.0 mbsf, 3.7° at 33.5 mbsf, 3.1° at 43.0 mbsf, and 3.0° at 52.5 mbsf. We pulled the bit above the seafloor at 1024 hr 12 April, and it cleared the rig floor at 1645 hr 12 April. We then recalled and recovered the beacon.

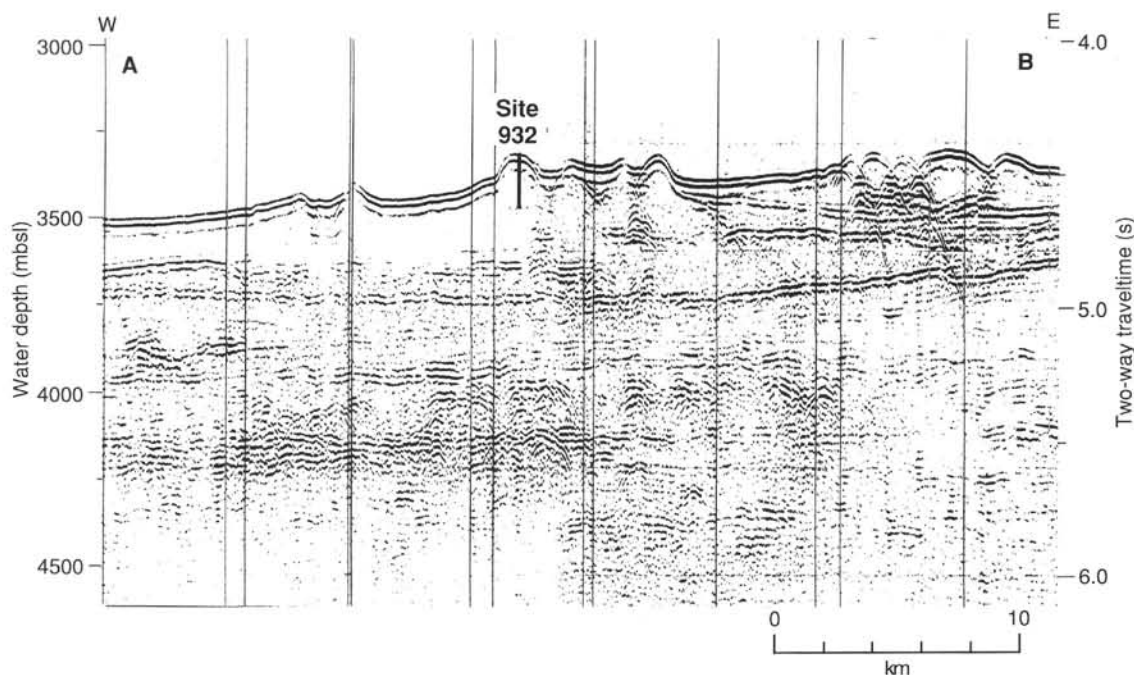


Figure 3. Seismic section through Site 932 (JOIDES Resolution, 0800–1155UTC on 5 April 1994).

## LITHOSTRATIGRAPHY

### Introduction

A total of 168.30 m of section was cored in two holes at Site 932 (Hole 932A, 0–168.30 mbsf, and Hole 932B, 0–52.50 mbsf) with high recovery (92% and 103%, respectively) in both holes (Fig. 4). Because the lithologies recovered in Hole 932B are nearly identical to those of Hole 932A, the following lithologic description is based mainly on cores from Hole 932A. Expansion of methane gas during core recovery commonly affected the sediment by disrupting the primary sedimentary structures in many silt and sand beds and by producing void spaces within many of the core sections. In addition, drilling disturbance formed drilling “biscuits” in some of the XCB cores, causing deformation and rotation of beds, which results in “chevron”- and “wood-grain”-like structures in the cores (see “Lithostratigraphy” section in the “Explanatory Notes” chapter, this volume). The sedimentary section is divided into two major lithologic units: Units I and II. Unit II is further subdivided into Subunits IIA and IIB (Fig. 4). The majority of the cored section is dark olive gray silty clay; discrete silt and sand laminae and beds are rare in Units I and IIA, but are common in Subunit IIB and increase in number and thickness downhole (Fig. 5). Unit II also contains rare thin intervals of disturbed or displaced sediment with deformed beds and mud clasts.

### Description of Lithostratigraphic Units

#### Unit I

Intervals: 155-932A-1H-1, 0–70 cm; 155-932B-1H-1, 0–62 cm  
Age: Holocene  
Depth: 0.00–0.70 mbsf

Unit I consists of brown (10YR 5/3) calcareous clay with abundant foraminifers and nannofossils. The sediment is moderately bioturbated and slightly color mottled. The carbonate content reaches a maximum of 42% in the upper 35 cm and decreases downward to 15% at the base of the unit (see “Organic Geochemistry” section, this chapter). This unit contains a distinctive dark reddish brown (5YR 4/

3) iron-rich crust (interval 155-932A-1H-1, 61–63 cm; 0.61–0.63 mbsf), which appears similar to crusts observed in the uppermost sediment at most of the other drill sites (e.g., Fig. 6 of “Site 930” chapter, this volume). Similar diagenetic, iron-rich crusts were analyzed previously and correlated throughout the Amazon Fan and adjacent Guiana Basin (e.g., Damuth, 1977; see “Introduction” chapter, this volume). Below this crust, Unit I is marked by a gradational color change to dark grayish brown (2.5Y 4/2) clay at the top of Subunit IIA. The lithostratigraphy of Unit I is similar to that observed in the uppermost sediment of the seafloor at most of the other drill sites.

#### Unit II

Intervals: 155-932A-1H-1, 70 cm, through -18X-CC, 24 cm; 155-932B-1H-1, 62 cm, through -6H-CC, 36 cm  
Age: Holocene to late Pleistocene  
Depth: 0.70–167.43 mbsf

Unit II includes the entire recovered section below Unit I in both holes and consists mainly of terrigenous dark olive gray (5Y 3/2) to very dark gray (5Y 3/1) silty clay. Most of the sediment in this unit is stained to varying degrees by diagenetic hydrotroilite, which imparts an ephemeral black color (N 2) to the sediment as irregular patches and/or color bands and laminae (e.g., Fig. 6; see “Introduction” chapter, this volume). In addition, burrow fills and micronodules (usually less than a few mm in diameter) stained by hydrotroilite are common to very abundant in some intervals. Grains in laminae and beds of silt and fine sand are also commonly stained black. The carbonate content is uniformly low throughout the entire unit and averages less than 3%. Unit II is subdivided into Subunits IIA and IIB based on the occurrence of silt and sand laminae and beds, and the gradational change from black color mottling to banding downhole.

#### Subunit IIA

Subunit IIA extends from Section 155-932A-1H-1 at 70 cm (0.70 mbsf) to -6H-2 at 150 cm (47.00 mbsf) and consists predominantly of dark olive gray (5Y 3/2) clay at the top that grades down to silty clay by 25 mbsf (Fig. 5). Black color mottling from hydrotroilite is extensive throughout the sediment below 1.40 mbsf and appears as very ir-

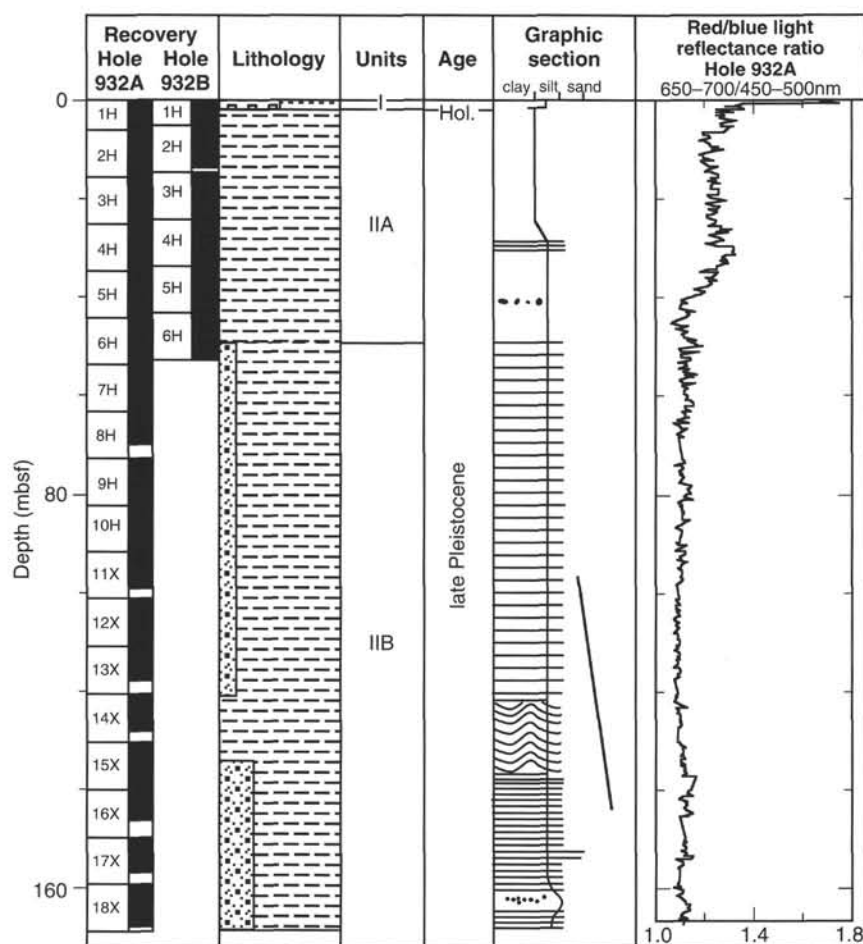


Figure 4. Composite stratigraphic section for Site 932 showing core recovery for both holes, a simplified summary of lithology for Hole 932A, depths of unit boundaries, age, a graphic section with generalized grain size and bedding characteristics, and downhole variations in light-reflectance values. The lithologic symbols are explained in Figure 1 of the "Explanatory Notes" chapter, this volume.

regular patterns, which appear to be associated with extensive bioturbation. In contrast, black color banding is rare to absent in this subunit. Laminae of silt and sand are very rare throughout this subunit (Fig. 5). Much of Subunit IIA is distinguishable from IIB by its higher spectral reflectance (Fig. 4).

A disturbed interval of sediment occurs from 40.81 to 42.10 mbsf (intervals 932A-5H-5, 31 cm, to -5H-6, 10 cm; 932B-5H-3, 133 cm, to -5H-4, 118 cm) and is composed of a contorted, plastically deformed and rarely folded mud matrix with numerous mud clasts of a variety of colors (shades of gray), shapes (well-rounded to angular), and sizes (less than 1 cm to 5 cm in diameter; average is ~2 cm; Fig. 7). An angular contact occurs at the base of this disturbed interval. This interval is interpreted as a mass-transport deposit that was probably replaced by a debris flow.

#### Subunit IIB

Subunit IIB extends from 47.00 to 168.30 mbsf (from Section 932A-6H-3, 0 cm, to -18X-CC, 24 cm; only the upper few meters of this unit were cored in Hole 933B (from Section 932B-6H-1, 100 cm, to -6H-CC, 36 cm). The sediment of this subunit consists of dark olive gray silty (5Y 3/2) clay at the top grading downhole into very dark gray (5Y 3/1) clay at approximately 95 mbsf. This subunit is characterized by the occurrence of discrete laminae and beds of silt and silt to fine sand (Fig. 5). Most of the sediment shows black, horizontal color bands or laminae spaced at intervals of approximately 1–3 cm. In some intervals, color bands are spaced closer than 1 cm and present a varve-like appearance (Fig. 6). The transition from Subunit IIA to IIB is gradational and is placed at the boundary between the color mottling and the color banding, just above the beginning of silt laminae (47.00 mbsf; Figs. 4 and 5).

The numerous, discrete silt laminae and silt-fine sand beds generally increase in frequency and thickness downhole (Figs. 5, 6A, and 8). Silt laminae increase from four in Core 932A-8H to approximately 75 in Core 932A-16X. Beds of silt and fine sand increase from one in Core 932A-6H near the top of the subunit to 22 in Core 932A-18X at the base of the subunit. Silt laminae are commonly <1–5 mm thick with most <3 mm thick (Fig. 6). Beds of silt and fine sand average 2–3 cm in thickness with a maximum thickness of 5 cm. Generally fewer than five beds per core occur downhole to approximately 130 mbsf (Fig. 5). The frequency and thicknesses of silt and fine sand beds increase markedly below 130 mbsf, where beds up to 15 cm thick occur at a frequency of up to 22 beds per core.

Although gas expansion appears to have disrupted the primary structures of many silt and fine sand beds, many beds do exhibit parallel or cross-lamination (Fig. 8). Many of the silt and fine sand beds, as well as some of the silt laminae, appear normally graded with sharp, irregular bases and gradational tops. Some grade upward from fine sand through silt into alternating laminae (~1 mm thick) of silt and mud, and finally into mud (Fig. 8).

A few intervals with disturbed sedimentary structures occur in Subunit IIB (Fig. 5). The thickest interval is 120.50 to 133.00 mbsf (from Section 932A-14X-1, 20 cm, to approximately -15X-2, 150 cm). Most of this interval down to -14X-CC, 23 cm, appears to show small-scale (i.e., less than the width of the core), rare convoluted folds; truncated laminae that dip in various directions and angles; and faulting (Fig. 9A). Because of XCB drilling disturbance this deformation resembles a "wood-grain" pattern (see "Lithostratigraphy" section in the "Explanatory Notes" chapter, this volume). The deformed structures are similar throughout the remainder of the interval, but are somewhat larger in scale, and commonly present a

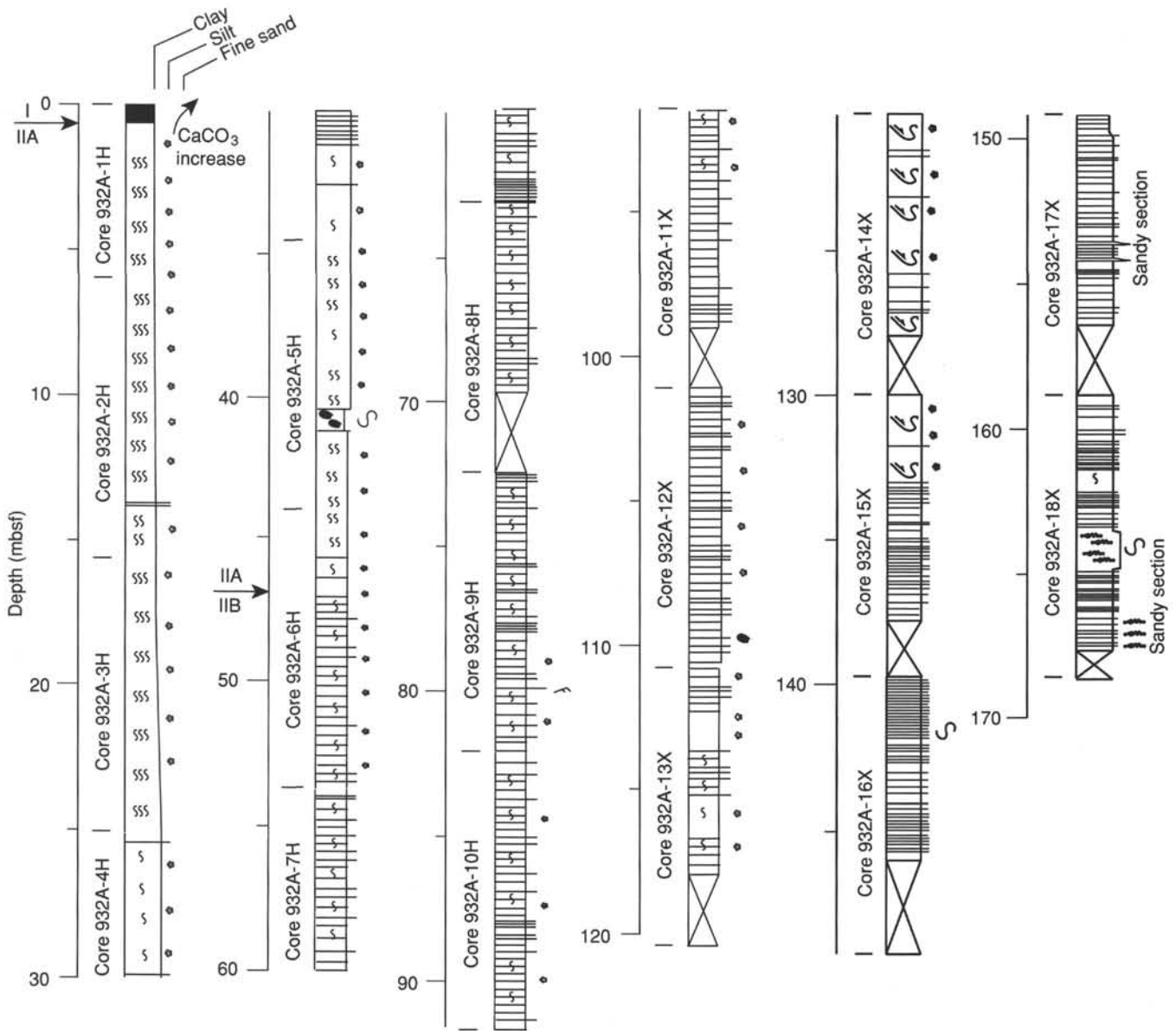


Figure 5. Graphic sedimentological columns for Site 932 showing grain-size variations (width of columns), bed thickness, and sedimentary structures; symbols and preparation of these columns are explained in the “Lithostratigraphy” section of the “Explanatory Notes” chapter, this volume. Arrows indicate the position of unit and subunit boundaries. The upper part of the column is shown in strike section of the foldout (back pocket, this volume) for comparison of levee sequences on the middle and upper fan.

“chevron” pattern (Fig. 9B). This deformed interval appears to represent sediment failure and subsequent decoupled, incremental movement by mass-transport processes, possibly slumping. Shorter intervals of similar sediment disturbance are observed in Sections 932A-16X-1, 0 cm, to -16X-2, 33 cm; interval 932A-18X-4, 22–145 cm; and interval 932A-12X-6, 98–108 cm. In each of these intervals, silt and sand laminae are disrupted or deformed.

**Mineralogy**

Mineralogy was determined by estimation of mineral volume percentages in smear slides and by X-ray diffraction (XRD) analysis of fine-grained silty clays.

**Smear-slide Synthesis**

The medium-to-coarse silt and fine sand of the silt and sand laminae and beds consist of relatively well sorted, angular grains of quartz (~40%), feldspar (~30%), micas (~15%) and accessory minerals (~15%). The accessory minerals include amphibole (mainly hornblende), augite and minor garnet, zircon, spinel, and monazite. The silt layers commonly contain a hydrotroilite-rich clay fraction (5% to 30%), which imparts the dark gray to black color of these layers. A silt lamina sampled in Subunit IIA (Sample 932B-4H-3, 100–101 cm) contained mixed biogenic and terrigenous silt-sized particles composed of 60% quartz and feldspars, 20% micas, and 20% foraminifer tests.

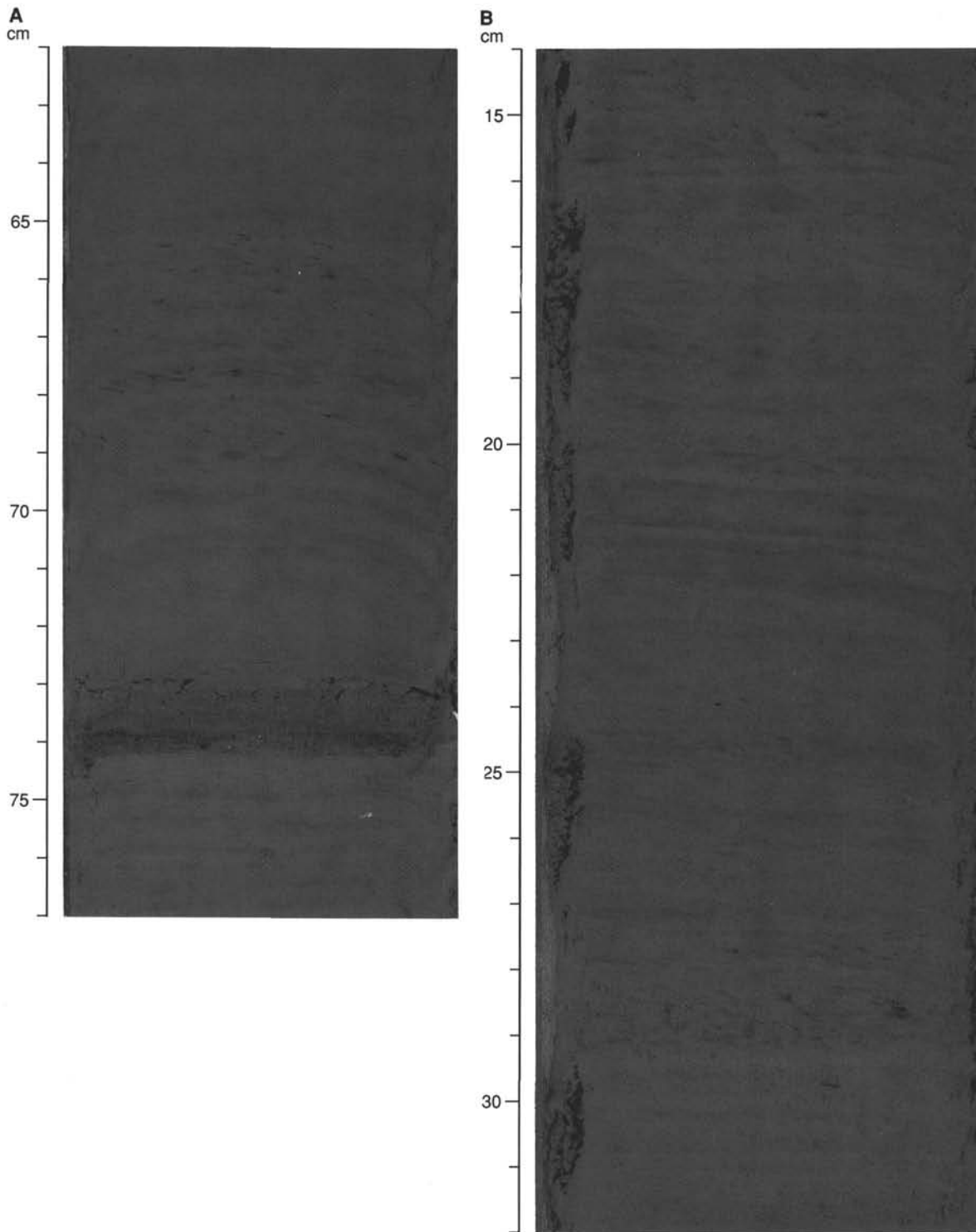


Figure 6. Examples of horizontal black color bands and laminations prevalent throughout Subunit IIB. **A.** Interval 155-932A-8H-7, 62–77 cm, showing examples of color laminations and bands. An example of a silt lamina is shown at 74 cm, which shows normal grading, sharp base, gradational top into mud, and internal parallel to cross-stratified laminations. **B.** Interval 155-932A-11X-5, 14–32 cm, showing color laminae on a scale of <1 cm. Note varve-like pattern.

The silty clays are composed of 70% clay minerals and 30% medium-to-fine silt (5 to 25 mm). The silt fraction is 65% quartz, 15%–20% feldspars, 10%–15% micas, and 5% accessory minerals dispersed in the clay or contained in thin laminae (0.25–1 mm thick). Diagenetic accessory minerals include widespread black hydrotroilite and blue-green vivianite. The feldspar and ferromagnesian minerals are very fresh, indicating rapid transport and burial.

#### *X-ray Diffraction Synthesis*

X-ray diffraction analysis was performed on bulk samples representing the dominant lithology from most cores recovered at Site 932 (Table 2). The most abundant minerals throughout the section are quartz, plagioclase, K-feldspar, augite, and the clay minerals smectite, illite (+ mica), and kaolinite. Quartz has the highest peak inten-

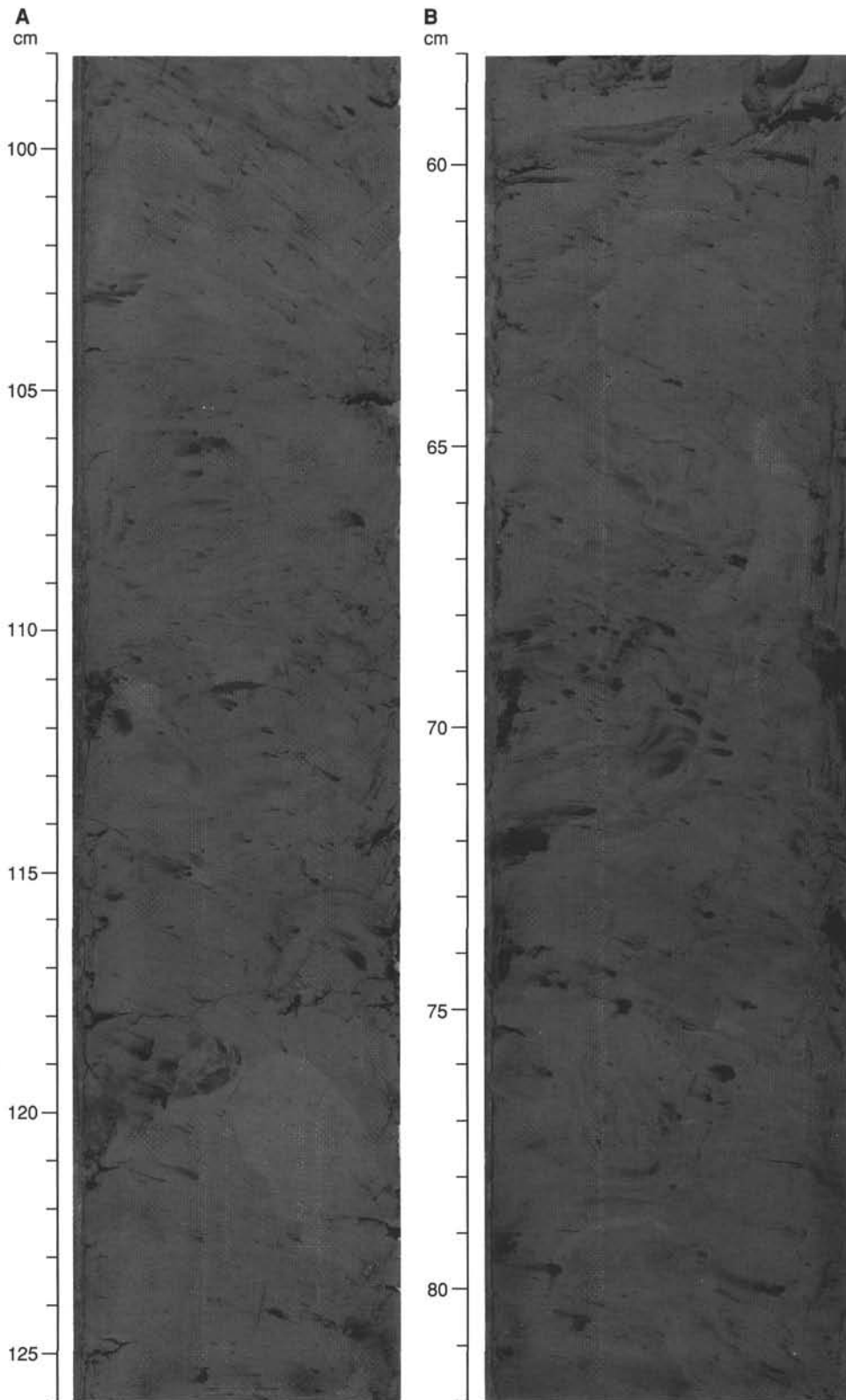


Figure 7. Examples of disturbed sediment from Subunit IIA showing mud clasts of various shapes, sizes, and colors, as well as deformed, flowed, folded, and faulted clay matrix. This sediment is interpreted as a debris-flow deposit. **A.** Interval 155-932A-5H-5, 98–126 cm. **B.** Interval 155-932B-5H-4, 58–82 cm.

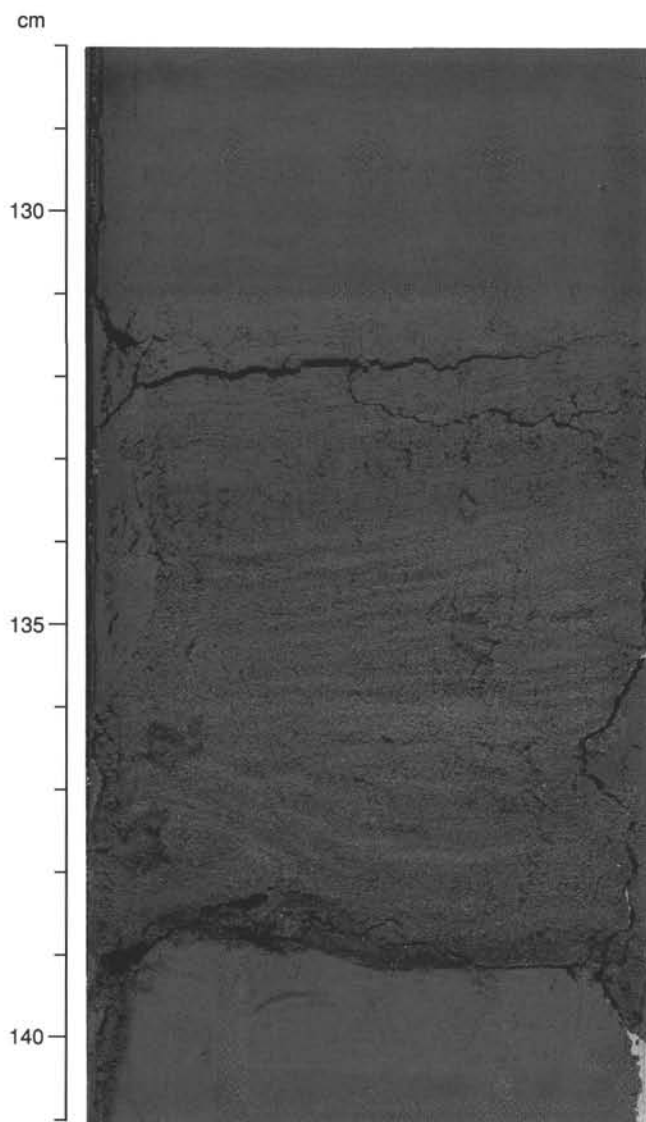


Figure 8. Example of a normally graded silt-fine sand bed from Subunit IIB (interval 155-932A-9H-6, 128-141 cm), showing sharp base, gradational top, and internal parallel to cross-stratified laminations.

sity. A few samples contain hornblende. When normalized to the intensity of the primary quartz peak, all clay minerals show variations in abundance down the section; however, the relationship of these variations to depositional history, if any, is uncertain.

### Spectrophotometry

Light-reflectance data reveal only minor changes throughout the sediment column recovered at Site 932. Light-reflectance levels are low (between 15% and 25% on average) because of the overall dark color (chroma) of the sediment. The ratio between the red and blue spectra (650–700 nm/450–500 nm) shows each lithologic unit or subunit is characterized by a distinctive ratio, which is probably determined by the ratio of iron oxyhydroxides to iron sulfides (Schneider et al., this volume). Spectral-reflectance data show that Subunit IIA is distinguishable from IIB by its higher reflectance in the red band (650–700 nm) that may be caused by a higher concentration of iron oxyhydroxides in this subunit than in Subunit IIB (Fig. 4).

## Discussion

Site 932 was drilled near the crest of the western levee of Channel-levee System 6B, which is one of the oldest channel-levee systems expressed in the seafloor morphology of the present-day fan surface. Because this channel has been inactive for many thousands of years, a section of hemipelagic deposits was expected to overlie the levee at the drill site. The recovered section at Site 932 apparently confirms this depositional history. Subunit IIB is a generally thinning- and fining-upward succession that apparently represents overbank deposition by turbidity currents. The frequency, thicknesses, and primary structures of the silt and silt to fine sand laminae and beds, coupled with the ubiquitous horizontal color banding and laminations of the clays, support this interpretation. Occasional failure of levee sediment may be responsible for deposition of sediment within the thin disturbed intervals, which appear to represent mass-transport deposits (e.g. slumps).

In contrast, Subunit IIA appears to represent hemipelagic deposition after the levee became inactive. Hemipelagic deposition is indicated by the presence of irregular color mottling, moderate to extensive bioturbation, very rare laminae and beds of silt and fine sand and mass-transport deposits. Alternation of zones of color mottling and banding near the boundary between Subunits IIA and IIB may record the nature and timing of the gradual transition from channel-levee activity to regional hemipelagic deposition. Hemipelagic deposits also appear to compose the sediment of Unit I; however, these carbonate-rich sediments apparently record the rather abrupt decrease in terrigenous sediment supply to the Amazon Fan in response to sea-level rise at the beginning of the Holocene (e.g., Damuth, 1977).

## BIOSTRATIGRAPHY

### Calcareous Nannofossils

The nannofossils at the mud line of Holes 932A and 932B have a highly diversified and well-preserved assemblage representing the upper part of the youngest nannofossil zone CN15b. The assemblages, which are dominated by *Emiliania huxleyi*, include common *Scyphosphaera* sp., *Helicosphaera kamptneri*, and *Ceratolithus cristatus*. The abundance and preservation of calcareous nannofossils quickly deteriorates below the “iron-rich crust” at a depth of 0.61 mbsf. The late-Pleistocene-age sections of both holes at Site 932 are either barren or contain a low abundance of nannofossils (Fig. 10; Table 3).

### Planktonic Foraminifers

In general, high abundance and a diverse assemblage of planktonic foraminifers are characteristic of Holocene sections, whereas low abundance and a lack of diversity are characteristic of upper Pleistocene sections. *G. tumida* is present only in the uppermost core catcher sample (Sample 932A-1H-CC, 10–19 cm) (Table 4). This places the boundary of the Ericson Z/Y zones between 6.10 and 15.52 mbsf. The Z/Y boundary is, however, most likely located near the base of Unit I, given the possible downhole contamination of the core catcher samples (Fig. 10; see discussion in the “Biostratigraphy” section, “Site 932” chapter, this volume). The *Y. p. obliq.* datum (40 ka) was based on the appearance of *P. obliquiloculata* at a depth of 44.9 mbsf in Hole 932A (Sample 932A-5H-CC, 45–54 cm), and at 43.9 mbsf in Hole 932B (Sample 932B-5H-CC, 41–50 cm).

### Benthic Foraminifers

Benthic foraminifers were found sporadically in Subunit IIA in Samples 932A-2H-CC, 20–29 cm (15.5 mbsf), 932B-3H-CC, 47–56

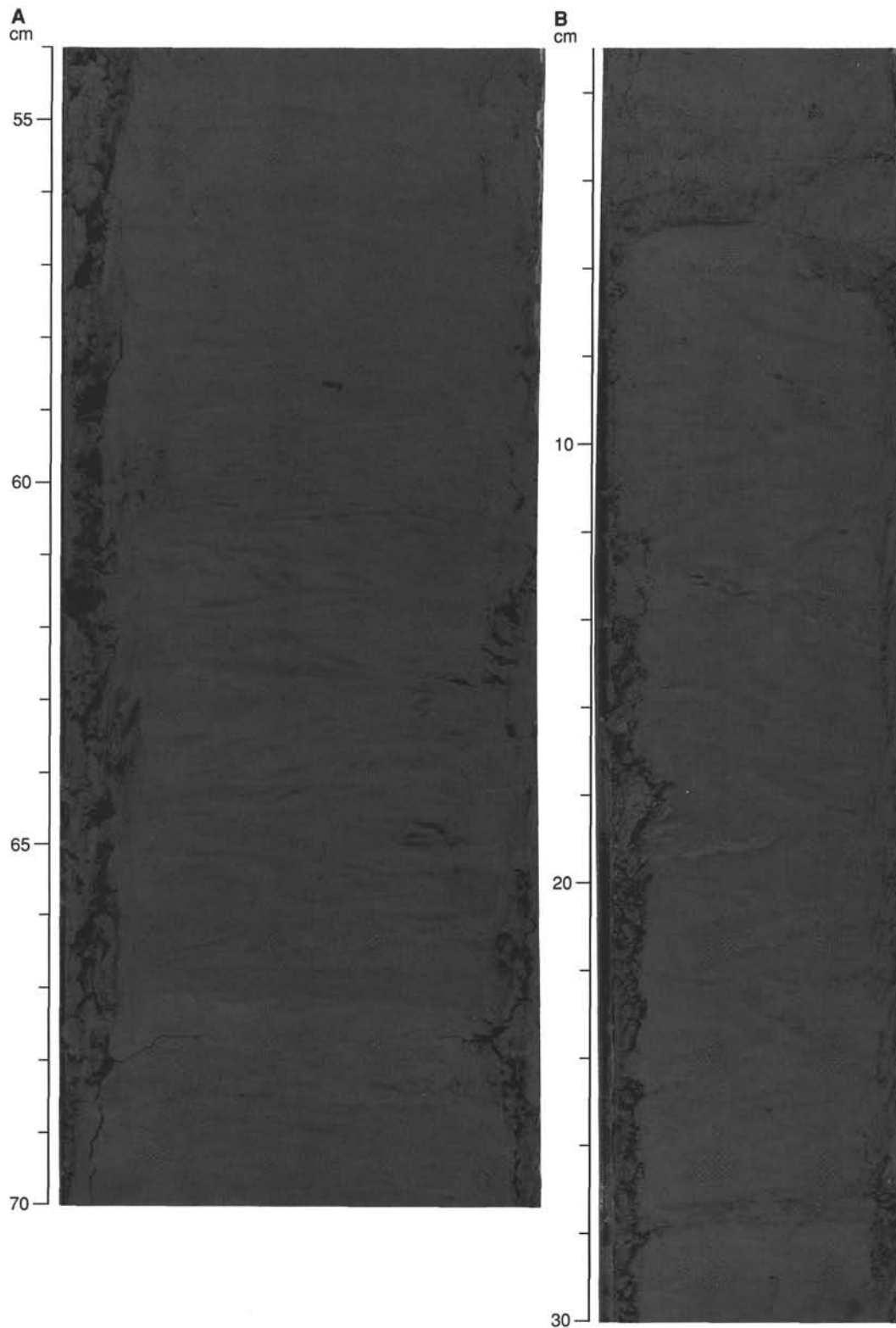


Figure 9. Examples of disturbed sediment from Subunit IIB, showing apparent folded, truncated beds that dip at various angles. **A.** Interval 155-932A-14X-1, 54–70 cm, showing “wood-grain” pattern produced by deformation. **B.** Interval 155-932A-15X-2, 1–30 cm, showing “chevron” pattern produced by drilling deformation (see “Lithostratigraphy” section, “Explanatory Notes” chapter, this volume). Deformation likely has been enhanced by XCB drilling disturbance. These sediments are interpreted as mass-transport deposits.

Table 2. Relative peak intensities of the main minerals in representative lithologies at Site 932.

Core, section, interval (cm)	Relative intensity of primary peaks								
	Smectite	Mica + Illite	Kaolinite	Quartz	Plagioclase	K-feldspar	Augite	Hornblende	Calcite
155-932A-									
1H-3, 68-69	9.6	29.3	16.0	100.0	9.8	10.3	3.3	*	*
2H-4, 50-52	9.7	23.3	11.5	100.0	11.7	5.0	2.6	*	*
3H-4, 50-51	13.0	29.0	15.1	100.0	11.2	*	3.0	*	*
4H-4, 49-50	15.3	31.4	15.8	100.0	11.6	4.0	2.6	2.6	*
5H-3, 58-59	14.6	40.1	18.6	100.0	9.9	*	3.5	*	*
7H-4, 50-51	12.8	37.3	15.7	100.0	8.0	8.6	8.0	2.9	*
8H-4, 49-50	11.9	27.6	15.9	100.0	10.8	*	2.4	*	*
9H-4, 45-46	8.7	16.3	9.1	100.0	8.5	3.8	1.9	*	*
10H-3, 80-81	14.9	29.8	14.6	100.0	10.4	4.5	2.8	*	*
11X-4, 44-45	12.5	30.8	15.4	100.0	9.3	4.5	3.0	*	*
11X-5, 10-12	17.5	30.1	18.3	100.0	9.7	4.7	3.6	3.3	*
12X-4, 50-51	13.3	24.0	13.1	100.0	7.5	7.5	3.3	2.6	*
13X-3, 55-56	10.4	21.0	14.6	100.0	8.6	4.8	2.7	*	*
14X-4, 36-37	10.4	17.4	12.5	100.0	8.3	*	3.1	*	*
15X-4, 36-37	12.5	25.4	13.8	100.0	9.1	3.1	2.4	*	*
16X-3, 43-44	14.2	30.2	17.3	100.0	12.6	7.7	2.9	*	*
17X-3, 61-62	19.5	34.2	16.2	100.0	11.8	*	2.5	*	*
18X-2, 58-59	14.9	26.0	15.3	100.0	10.0	*	2.1	*	*

Notes: See "Lithostratigraphy" section in "Explanatory Notes" chapter, this volume, for XRD methods. \*denotes non-detection.

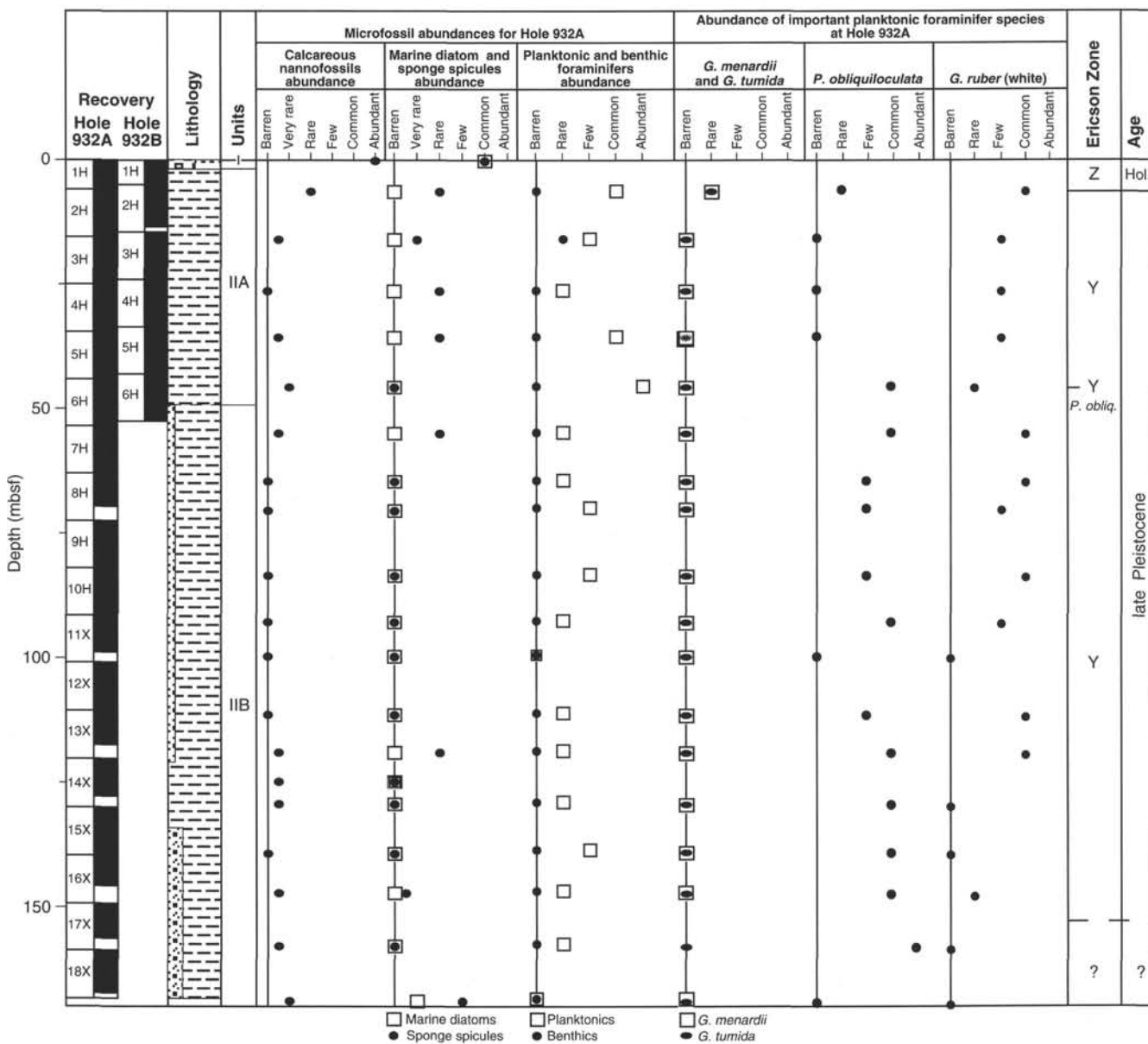


Figure 10. Biostratigraphic summary for Site 932.

Table 3. Calcareous nannofossil and siliceous microfossil abundance data for Holes 932A and 932B.

Core, section, interval (cm)	Top interval (mbsf)	Bottom interval (mbsf)	Calcareous nannofossils			Diatoms		Sponge spicules	Radiolarians	Ericson Zone (inferred from foraminifers)	Age (inferred from foraminifers)
			Abundance	Preservation	Zone	Marine	Fresh water				
155-932A-											
1H-MI, 0-0	0.00	0.00	a	g	CN15b	c	r	c	r	Z	Holocene
1H-CC, 19-20	6.19	6.20	r	p	—	b	b	r	b	Y	late Pleist.
2H-CC, 29-30	15.61	15.62	tr	—	—	b	b	vr	b	Y	late Pleist.
3H-CC, 39-40	25.99	26.00	b	—	—	b	b	r	b	Y	late Pleist.
4H-CC, 31-32	35.14	35.15	tr	—	—	b	b	r	b	Y	late Pleist.
5H-CC, 54-55	44.92	44.93	vr	p	—	b	b	b	b	Y <sub>P. obliq.</sub>	late Pleist.
6H-CC, 35-36	54.28	54.29	tr	—	—	b	b	r	b	Y	late Pleist.
7H-CC, 48-49	63.86	63.87	b	—	—	b	b	b	b	Y	late Pleist.
8H-CC, 104-105	69.46	69.47	b	—	—	b	b	b	b	Y	late Pleist.
9H-CC, 87-88	82.63	82.64	b	—	—	b	b	b	b	Y	late Pleist.
10X-CC, 37-38	91.74	91.75	b	—	—	b	b	b	b	Y	late Pleist.
11X-CC, 25-26	98.76	98.77	b	—	—	b	b	b	b	—	—
12X-CC, 21-22	110.42	110.43	b	—	—	b	b	b	b	Y	late Pleist.
13X-CC, 35-36	117.62	117.63	tr	—	—	b	b	r	b	Y	late Pleist.
14X-3, 13-14	123.43	123.44	tr	—	—	b	b	b	b	Y	late Pleist.
14X-3, 16-17	123.46	123.47	tr	—	—	b	b	b	b	Y	late Pleist.
14X-CC, 22-23	127.85	127.86	tr	—	—	b	b	b	b	Y	late Pleist.
15X-CC, 24-25	137.74	137.75	b	—	—	b	b	b	b	Y	late Pleist.
16X-CC, 26-27	145.78	145.79	tr	—	—	b	b	tr	b	Y	late Pleist.
17X-CC, 44-45	156.22	156.23	tr	—	—	b	b	b	b	?	?
18X-CC, 23-24	167.42	167.43	vr	p	—	vr	vr	f	b	?	?
155-932B-											
1H-CC, 14-15	5.04	5.05	tr	—	—	b	b	b	b	Y	late Pleist.
2H-CC, 33-34	13.51	13.52	tr	—	—	b	b	f	b	Y	late Pleist.
3H-CC, 56-57	24.38	24.39	tr	—	—	b	b	r	b	Y	late Pleist.
4H-CC, 26-27	33.92	33.93	tr	—	—	b	b	b	b	Y	late Pleist.
5H-CC, 50-51	43.94	43.95	vr	p	—	b	b	tr	b	Y <sub>P. obliq.</sub>	late Pleist.
6H-CC, 35-36	53.30	53.31	vr	p	—	b	r	f	—	Y	late Pleist.

cm (24.4 mbsf), and 932B-5H-CC, 41-50 cm (43.9 mbsf) (Table 4). The benthic foraminifers found in these samples are from the deep-water, low-oxygen abyssal group comprising *Uvigerina* spp. and *Pyrgo* spp. This suggests that within the first 44 mbsf there were periods of time when the sedimentation was low enough to permit an in-situ benthic community.

### Siliceous Microfossils

At Site 932 low abundances of both freshwater and marine diatoms were observed (Table 3). Pelagic diatoms of marine origin are rare but well preserved in the mud-line sample of Hole 932A. The assemblage includes, among others, *Nitzschia* sp., a number of species from the genera *Coscinodiscus*, and *Actinocyclus* sp. The freshwater diatoms present in the mud-line sample are represented by chains of well-preserved specimens of *Melosira granulata*. In Hole 932A, diatom abundance decreases rapidly downhole, and diatoms are absent except in the bottom of Hole 932A (Sample 932A-18X-CC, 23-24 cm), where the freshwater diatom *Melosira granulata* appears together with rare fragments of marine pelagic diatoms. In Hole 932B, freshwater diatoms were observed in smear slides from Sample 932B-6H-CC, 35-36 cm. Siliceous sponge spicules occurred throughout the drilled sequences of Site 932 (Table 3; Fig. 10).

### Palynology

Palynomorph abundance and preservation vary downhole in Holes 932A and 932B. In general, high abundance, good preservation, and relatively high diversity is characteristic only in the Pleistocene section. In contrast, the Holocene section is mostly barren (Table 5). Detailed examination of closely spaced samples from Core 932A-1H through -3H (Table 5) reveals a pollen and spore assemblage that may represent glacial conditions, based on foraminifer age determinations. The major pollen types observed from this sediment include Euphorbiaceae, Rhizophoraceae, Gramineae, Cyperaceae, and tricolporate (TCP), tricolpate (C), and stephanoporate (SP) types. Fern spores include Cyatheaceae, Lycopodiidae, and monolete types. A second group of samples was examined from the *Y<sub>P. obliq.</sub>* datum

level (Samples 932A-5H-CC, 54-55 cm; 932B-6H-4, 64-66 cm; 932B-6H-7, 8-10 cm; and 932B-6H-CC, 35-36 cm), which is approximately 40 ka, and may represent a slightly warmer period during a glacial (isotopic Stage 3). Major pollen types include tricolporate (TCP) and tricolpate (C) types, and Cyperaceae. Fern spores include Cyatheaceae, trilete spores, and monolete spores. The pollen and spore assemblage from around the *Y<sub>P. obliq.</sub>* datum (40 ka) level contain lower abundances and diversities than the samples of late Pleistocene age. The changing pollen and spore abundances at three different sea-level stages show a clear decrease in pollen and spore abundance at Hole 932A as sea level rises (Fig. 11). The abundance of pollen and spores is most likely influenced by a number of factors linked to changing sea level, including sediment transport paths, wind direction, surface currents, and the shoreline proximity. Varying abundances of wood particles have been observed in all palynology slides examined. Dinoflagellates are rare or absent in the samples examined and appear to be poorly preserved in the Amazon Fan sediment.

### Stratigraphic Summary

Calcareous and siliceous microfossil groups occur in high abundances in the brown nannofossil foraminifer clay of Unit I recovered at the top of Holes 932A and 932B. This section has been classified as Zone Z or Holocene. The disappearance of *G. menardii* and *G. tumida* from the foraminifer assemblage places the Ericson Z/Y boundary below the first core catcher sample at a depth of 6.1 mbsf (Sample 932A-1H-CC, 10-19 cm). The Z/Y boundary is, however, most likely located at a shallower depth close to the base of Unit I, given the possible downhole contamination of core catcher samples. Below this section microfossils occur in low abundances in the dark olive to dark grey silty clay. The *Y<sub>P. obliq.</sub>* datum (40 ka) occurs at a depth of 44.9 mbsf in Hole 932A, and 43.9 mbsf in Hole 932B. Pollen and spores were found to be common to abundant in the upper Pleistocene section and almost absent in the Holocene. The abundance of pollen and spores appears to be strongly influenced by changing transport processes at different sea-level stages.

Table 4. Foraminifer abundance data for Holes 932A and 932B.

Core, section, interval (cm)	Top interval (mbsf)	Bottom interval (mbsf)	<i>Globorotalia menardii</i>	<i>Globorotalia tumida</i> (left)	<i>Globorotalia tumida</i> (right)	<i>Globorotalia tumida flexuosa</i>	<i>Pulleniatina obliquiloculata</i>	<i>Globigerinoides ruber</i> (white)	<i>Globigerinoides ruber</i> (pink)	<i>Globorotalia hexagonus</i>	<i>Neogloboquadrina duterrei</i>	<i>Globorotalia trilobus trilobus</i>	<i>Globorotalia inflata</i>	<i>Globorotalia truncatulinoides</i> (left)	<i>Globorotalia truncatulinoides</i> (right)	<i>Globigerina bulloides</i>	<i>Globigerinella trilobus saccullifer</i>	<i>Globigerinella aequilateralis</i>	<i>Orbulina universa</i>	<i>Globigerinita glutinata</i>	<i>Globigerinoides conglobatus</i>	<i>Globoquadrina conglomera</i>	<i>Neogloboquadrina pachyderma</i> (right)	<i>Neogloboquadrina pachyderma</i> (left)	<i>Globigerina quinqueloba</i>	<i>Globigerina rubescens</i>	<i>Globorotalia scintila</i>	<i>Globorotalia tosaensis</i>	Other planktonic foraminifers	Overall foraminifer abundance	Preservation	Abundance of benthic foraminifers	Ericson Zone	Age			
155-932A-																																					
1H-CC, 10-19	6.10	6.19	R	R	B	B	R	C	R	B	C	C	B	B	F	B	F	B	B	B	R	R	B	B	B	B	B	B	B	R	C	M	B	Y	late Pleist.?		
2H-CC, 20-29	15.52	15.61	B	B	B	B	B	F	C	B	C	C	B	B	B	F	B	C	B	B	B	B	B	B	B	B	B	B	B	R	F	M	R	Y	late Pleist.		
3H-CC, 30-39	25.90	25.99	B	B	B	B	B	F	R	B	B	C	C	B	B	C	B	B	B	B	B	B	B	B	B	B	B	B	B	R	C	M	B	Y	late Pleist.		
4H-CC, 22-31	35.05	35.14	B	B	B	B	B	F	R	B	B	C	C	C	B	B	C	B	F	R	R	B	B	B	B	B	B	B	B	R	C	M	B	Y	late Pleist.		
5H-CC, 45-54	44.83	44.92	B	B	B	B	C	R	F	B	C	C	C	B	B	C	B	R	F	B	B	R	R	B	B	B	B	B	B	R	A	M	B	Y <sub>P.obliq.</sub>	late Pleist.		
6H-CC, 26-35	54.19	54.28	B	B	B	B	C	C	C	B	B	F	F	B	B	C	B	F	B	B	B	B	B	B	B	B	B	B	B	B	R	G	B	Y	late Pleist.		
7H-CC, 39-48	63.77	63.86	B	B	B	B	F	C	B	B	C	B	B	B	C	B	B	B	B	B	B	B	B	B	B	B	B	B	B	R	R	M	B	Y	late Pleist.		
8H-CC, 95-104	69.37	69.46	B	B	B	B	F	C	F	B	B	C	C	B	B	F	B	F	B	B	B	B	B	B	B	B	B	B	B	B	F	G	B	Y	late Pleist.		
9H-CC, 78-87	82.54	82.63	B	B	B	B	F	C	R	B	F	C	B	B	C	B	F	B	B	B	B	B	B	B	B	B	B	B	B	R	F	G	B	Y	late Pleist.		
10X-CC, 28-37	91.65	91.74	B	B	B	B	C	F	F	B	B	C	F	B	B	F	B	B	F	R	B	B	B	B	B	B	B	B	B	R	B	M	B	Y	late Pleist.		
11X-CC, 16-25	98.67	98.76	B	B	B	B	B	B	B	B	B	B	B	B	B	B	B	B	B	B	B	B	B	B	B	B	B	B	B	B	B	B	B	B	—	—	—
12X-CC, 12-21	110.33	110.42	B	B	B	B	C	C	B	B	C	C	C	B	B	C	B	B	B	B	B	B	B	B	B	B	B	B	B	B	R	G	B	Y	late Pleist.		
13X-CC, 26-35	117.53	117.62	B	B	B	B	F	C	C	B	B	C	F	B	B	C	B	F	B	B	B	B	B	B	B	B	B	B	B	B	R	M	B	Y	late Pleist.		
14X-CC, 13-22	127.76	127.85	B	B	B	B	C	B	B	B	C	C	C	B	B	B	B	C	B	B	B	B	B	B	B	B	B	B	B	B	R	M	B	Y	late Pleist.		
15X-CC, 15-24	137.65	137.74	B	B	B	B	C	B	B	B	C	B	B	B	B	F	B	C	B	B	B	R	B	B	B	B	B	B	B	B	F	M	B	Y	late Pleist.		
16X-CC, 17-26	145.69	145.78	B	B	B	B	C	R	B	B	B	A	R	B	B	B	B	R	R	B	B	B	B	B	B	B	B	B	B	B	R	G	B	Y	late Pleist.		
17X-CC, 35-44	156.23	156.22	F	B	B	B	A	B	B	B	B	B	B	B	B	A	B	B	B	B	B	F	B	B	B	B	B	B	B	B	R	M	B	?	?		
18X-CC, 14-23	167.33	167.42	B	B	B	B	B	B	B	B	B	B	B	B	B	B	B	B	B	B	B	B	B	B	B	B	B	B	B	B	B	—	B	?	?		
155-932B-																																					
1H-CC, 5-14	4.95	5.04	R	B	B	B	F	C	B	B	C	B	B	B	C	B	F	B	B	B	B	B	R	B	B	B	B	B	B	R	C	G	B	Y	late Pleist.		
2H-CC, 24-33	13.42	13.51	B	B	B	B	B	A	B	B	A	B	B	B	B	B	B	B	B	B	B	B	B	B	B	B	B	B	B	B	R	P	B	Y	late Pleist.		
3H-CC, 47-56	24.29	24.38	B	B	B	B	B	C	B	B	C	B	B	B	B	C	B	B	B	B	B	B	B	B	B	B	B	B	B	B	R	P	R	Y	late Pleist.		
4H-CC, 17-26	33.83	33.92	B	B	B	B	F	B	B	B	B	B	B	B	B	B	B	B	B	B	B	B	B	B	B	B	B	B	B	B	B	—	B	Y	late Pleist.		
5H-CC, 41-50	43.85	43.94	B	B	B	B	F	C	B	B	C	B	B	B	B	C	B	F	B	R	B	B	B	B	B	B	B	B	B	B	R	B	M	R	Y <sub>P.obliq.</sub>	late Pleist.	
6H-CC, 26-35	53.21	53.30	B	B	B	B	C	C	F	B	C	B	B	B	B	B	B	B	B	B	B	B	B	B	B	B	B	B	B	B	R	M	B	Y	late Pleist.		

Table 5. Palynomorph abundance and type data for Holes 932A and 932B.

Core, section, interval (cm)	Top interval (mbsf)	Bottom interval (mbsf)	Pollen and spores			Dinocysts	Wood/ carbonized particles	Ericson zone (inferred from forams.)	Age (inferred from forams.)
			Abundance	Preservation	Major types recorded				
155-932A-									
1H-1, 44-46	0.44	0.46	b			r	r	Z	Holocene
1H-3, 44-46	3.44	3.46	a	g	SP, TC, Gramineae, Cyatheaceae, monolete (psilate) spore	b	c	Y	late Pleist.
2H-2, 51-55	8.01	8.05	c	g	Rhizophora, Mauritia (?), Cyatheaceae, Euphorbiaceae	b	a	Y	late Pleist.
2H-4, 67-71	11.17	11.21	a	m	Alnus, TCP, Gramineae, monolete (psilate) spore	b	c	Y	late Pleist.
2H-6, 34-36	13.84	13.86	c	m	Gramineae, Cyatheaceae	b	c	Y	late Pleist.
3H-1, 54-56	16.04	16.06	c	m	Alnus, Gramineae, Cyatheaceae	r	c	Y	late Pleist.
3H-3, 143-145	19.93	19.95	a	m	TCP, TC, Cyatheaceae, Lycopodiidae	b	a	Y	late Pleist.
3H-6, 45-47	23.45	23.47	c	g	Euphorbiaceae, TCP	b	c	Y	late Pleist.
5H-CC, 54-55	44.92	44.93	r	g	TC	b	a	Y <sub>p. obliq.</sub>	late Pleist.
155-932B-									
6H-4, 64-66	48.14	48.16	a	m	TCP, Cyatheaceae, monolete spore	b	c	Y <sub>p. obliq.</sub>	late Pleist.
6H-7, 8-10	52.08	52.10	f	m	Cyperaceae, monolete spore	b	c	Y <sub>p. obliq.</sub>	late Pleist.
6H-CC, 35-36	53.30	53.31	f	m	TCP, Cyatheaceae, trilete spore	b	c	Y <sub>p. obliq.</sub>	late Pleist.

Notes: SP = stephanoporate; TCP = tricolporate; TC = tricolpate.

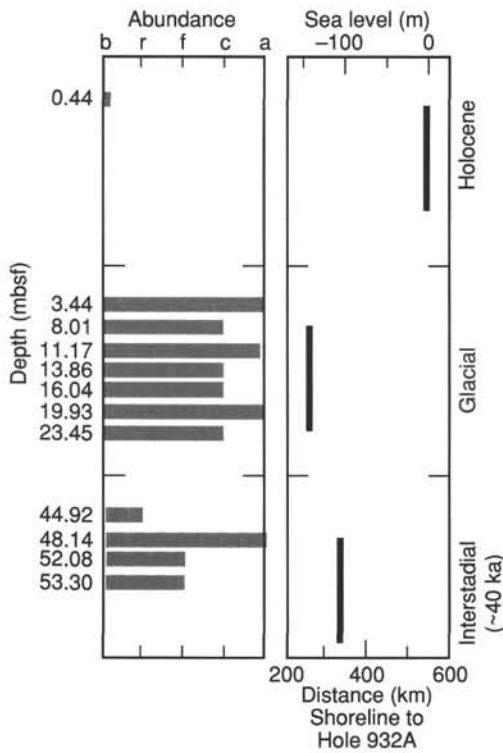


Figure 11. Pollen and spore abundance in relation to different sea levels (distance from source vegetation).

### PALEOMAGNETISM Remanence Studies

Measurements on the archive halves of all 15 APC cores and of four XCB cores from this site were made using the pass-through magnetometer. The Tensor tool was employed on Cores 932A-3H through -7H and -9H, and Cores 932B-3H through -6H. The tool continued to function well as the corrected declinations were generally distributed near to 0°.

Azimuthally uncorrected declinations for the APC cores appear to be randomly distributed from core to core (Fig. 12), an indication that the remanence acquired during drilling or core recovery was not biasing the magnetization vectors to any significant extent. However, declination values tend to decrease (i.e., swing to the west) downhole

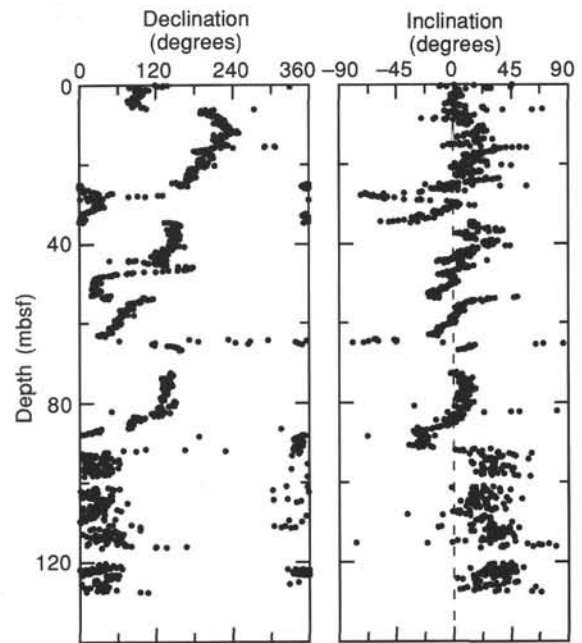


Figure 12. Magnetic declination (uncorrected) and inclination, after AF demagnetization to 25 mT, for all Hole 932A archive-half cores measured on the pass-through cryogenic magnetometer.

within individual APC cores. This swing probably results from counter-clockwise rotation of the sediment within the core barrel during recovery. In addition, a few of the APC cores show a progression toward less positive inclination values downcore suggesting enhanced drill stem remanence acquisition toward the top of the core.

We are more concerned with the strong bias of AF demagnetized declination values toward 0° for the XCB cores (below 92 mbsf in Fig. 12). This tendency, along with consistently positive inclination values, suggests that a drilling-induced remanence remained in the Site 931 XCB cores even after AF demagnetization to 25 mT. The natural remanent magnetizations (NRMs) of seven discrete samples from this interval had declinations distributed about 180°. These antipodal declinations may indicate a radially inward component of magnetization, similar to that encountered during Leg 154 (Curry, Shackleton, Richter, et al., in press). However, in our case, AF demagnetization to 40 mT resulted in a significant rotation of the declinations for the discrete samples away from this preferred direction.

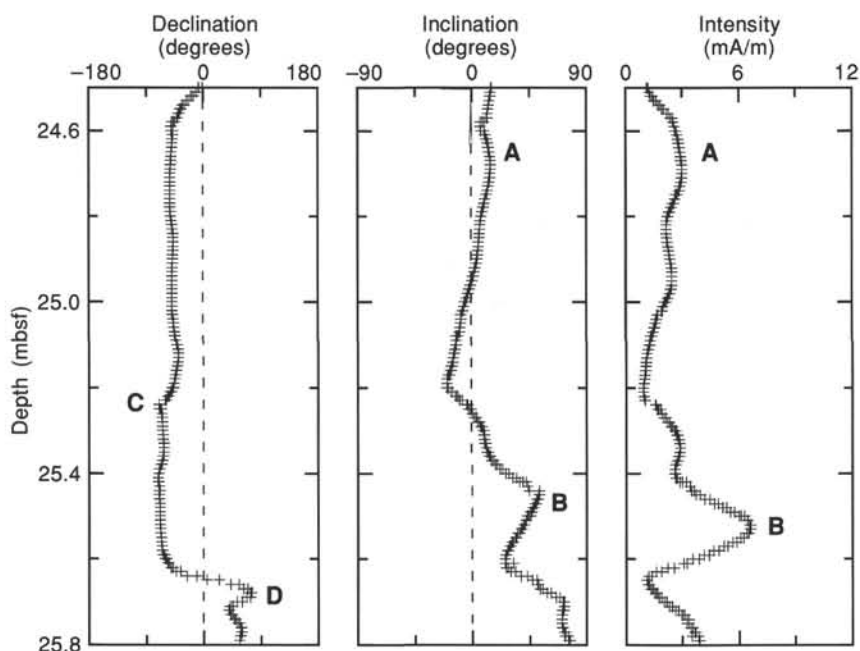


Figure 13. Declination, inclination, and intensity for an apparent geomagnetic excursion (Lake Mungo Excursion? at ~30 ka) recorded in archive-half Section 155-932A-3H-7 and top of the core catcher. Measurement interval was 0.5 cm, after AF demagnetization to 27 mT. A, B, C, and D refer to characteristic features similar to those seen in the Site 930 excursion records (see Figs. 18 and 19 of "Site 930" chapter, this volume). Declination values have been corrected using Tensor tool data. Spurious flux jumps in the magnetometer's Y axis have been removed from the declination data.

The paleomagnetic excursion (Lake Mungo(?) at ~30 ka), first noted at Site 930, is identified in Section 932A-3H-7 on the basis of the distinctive changes in remanence direction and intensity (Fig. 13). As with Site 930, the stratigraphic position of the excursion is consistent with the occurrence of the foraminifer *P. obliquiloculata* in Core 932A-5H. This paleomagnetic event is not seen in its entirety in Hole 932A due to incomplete recovery in Section 932A-3H-7.

A clear oscillatory pattern in declination is observed in Sections 932A-4H-5, -6, and -7 and throughout Core 932A-5H (Fig. 14). Nine cycles are identifiable, spanning a depth range of 31.5 to 44 mbsf, or 12.5 m. This interval corresponds to a zone of mostly homogeneous dark silty clay in which discrete silt laminae are absent.

### Magnetic Susceptibility

Whole-core and discrete-sample magnetic susceptibility indicate generally uniform susceptibility values within Subunits IIA and IIB (Fig. 15).

## ORGANIC GEOCHEMISTRY

### Volatile Hydrocarbons

Headspace methane concentrations at Site 932 increase rapidly below the sediment surface to a maximum value of 38,700 ppm at 13.50 mbsf (Table 6; Fig. 16). Below this depth, methane concentrations decrease continuously to 4830 ppm at 161.7 mbsf. There is a spike (12,400 ppm) in headspace methane concentration at 116.55 mbsf, which is also observed in the vacutainer sample. As at previous sites, vacutainer methane values are much higher than headspace concentrations (Fig. 16). Methane concentrations greater than 600,000 ppm are measured between 42.00 mbsf and 80.89 mbsf with a maximum value at 51.50 mbsf. Higher molecular weight hydrocarbons were not detected, indicating a predominantly biogenic methane source at Site 932.

### Carbon, Nitrogen, and Sulfur Concentrations

Calculated  $\text{CaCO}_3$  concentrations are high in the top 0.7 mbsf, ranging from 42% to 15% (Table 7; Fig. 17). They are much lower

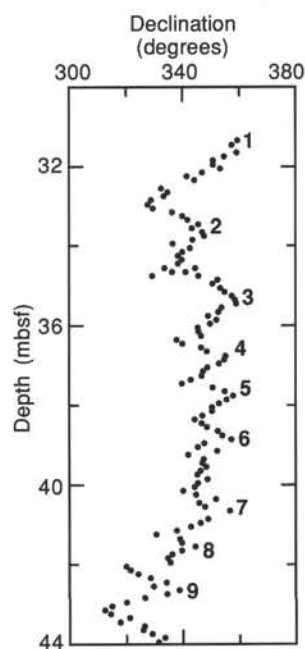


Figure 14. Oscillations in the declination record (numbered sequentially) within archive-half Cores 932A-4H and -5H. Measurements were made on the pass-through cryogenic magnetometer after AF demagnetization to 25 mT. Measurement interval was 10 cm. Declinations are corrected using Tensor tool data.

(<3%) throughout the rest of Hole 932A, except for somewhat elevated values at 19.15 mbsf (6.6%), 20.93 mbsf (5.7%), and 61.50 mbsf (5.5%). TOC concentrations are low (<0.5%) above 0.7 mbsf and steadily increase below this depth to about 1.1% at 49.60 mbsf (Table 7; Fig. 17). In the interval between 49.60 and 125.28 mbsf, most TOC concentrations range between 1.15% and 0.85%. Several silt and sand layers including those at 62.68, 79.26, 135.04, 136.10, 141.90 mbsf, display markedly lower TOC concentrations (<0.6%; Fig. 17).

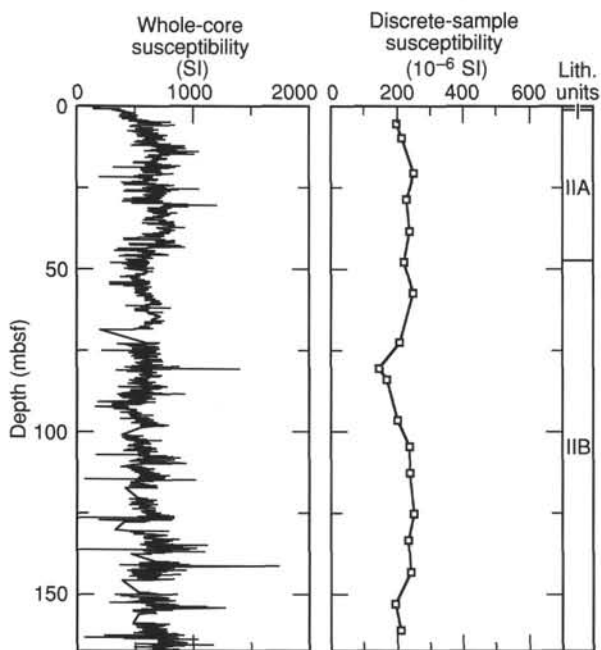


Figure 15. Whole-core and discrete-sample magnetic susceptibilities for Hole 932A.

Table 6. Gas concentrations in sediments from Site 932.

Core, section, interval (cm)	Depth (mbsf)	Sed. temp.* (°C)	Methane	
			HS (ppm)	VAC (ppm)
155-932A-				
1H-4, 0-5	4.50	2	24	
2H-6, 0-5	13.50	2	38,718	
3H-6, 0-5	23.00	3	24,827	
4H-6, 0-5	32.50	3	15,111	151,000
5H-6, 0-5	42.00	3	15,074	604,161
6H-6, 0-5	51.50	4	8,958	740,136
7H-7, 0-5	62.50	4	6,184	699,256
8H-CC, 0-5	68.42	4	7,415	
9H-7, 0-5	80.89	4	6,763	673,110
11X-5, 0-5	97.24	5	4,992	19,294
12X-5, 0-5	107.00	5	6,800	
13X-5, 0-5	116.55	6	12,408	538,985
14X-5, 0-5	126.30	6	6,969	17,220
15X-4, 0-5	134.50	6	6,720	
16X-4, 0-5	144.20	6	7,216	
17X-3, 0-5	152.20	7	4,950	
18X-3, 0-5	161.70	7	4,830	71,536

Notes: HS = Headspace; VAC = Vacutainer. Geothermal gradient = 31°C/km. Bottom-water temperature = 2°C. \*See "In-situ Temperature Measurements" section, this chapter.

Total nitrogen concentrations range between 0.05% and 0.11% in Hole 932A and show a similar profile to TOC (Fig. 17). TS concentrations are low (0% to 0.18%) throughout the hole except for two higher values at 11.45 mbsf (3.28%) and 44.60 mbsf (4.17%). These samples were taken in sediment sections with high abundances of iron sulfide.

Samples with high CaCO<sub>3</sub> concentrations were taken from the brown calcareous clay Unit I (see "Lithostratigraphy" section, this chapter), as at previous sites. Low TOC concentrations (<0.5%) characteristic of this section most likely reflect lower terrigenous input. Low TOC (<0.4%) and TN (<0.06%) values are observed in several samples from sand and silt layers of Unit II (Fig. 17), indicating a relationship similar to that observed in previous sites.

Atomic ratios of organic carbon to total nitrogen, [C/N]<sub>a</sub>, in the top 0.70 mbsf are generally low (<10) and increase with depth to values ranging from 8 to 14. [C/N]<sub>a</sub> ratios greater than 15 were found at 109.00 and 109.50 mbsf. No trend in [C/N]<sub>a</sub> with depth is seen.

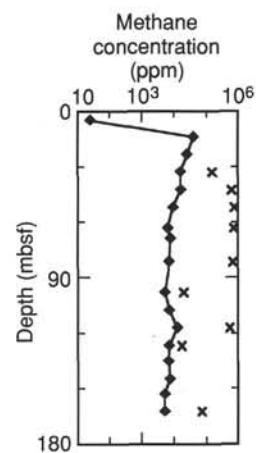


Figure 16. Methane concentrations (ppm) at Site 932. Headspace (diamond) and vacutainer (x) samples are plotted.

### Rock-Eval Data

Hydrogen index data were determined from Rock-Eval analyses of selected sediment samples (Table 8). All the sediment yields very low (<60) HI values, indicating a predominantly terrigenous source for the organic matter present throughout Hole 932A.

## INORGANIC GEOCHEMISTRY

### Interstitial Water Analysis

Interstitial water analyses were performed on nine sediment samples from Hole 932A. Samples were taken approximately every 10 m for the upper 42 mbsf and approximately one per 30 m thereafter. The analytical results are shown in Table 9 and Figure 18.

Salinities of the water samples range from 32.0 to 35.5 (Fig. 18A). The shallowest sample, at 4.45 mbsf has the highest salinity, 35.5. Below 4.45 mbsf, salinity is fairly uniform between 32 and 33. The salinity decrease is due to loss of dissolved sulfate, through sulfate reduction, and loss of magnesium and calcium, presumably to carbonate mineral precipitation.

Chloride concentrations increase steadily in the upper 40 m of the hole, from 552 mM at 4.45 mbsf to 563 mM at 41.95 mbsf. The values then remain between 563 and 560 mM through the rest of the hole (Fig. 18B). The downhole increase may represent preserved high chlorinity, paleo-pore waters in the pre-Holocene sediment.

Pore-water pH values range from 7.39 to 7.79. There is a downhole trend toward higher values (Fig. 18C).

Pore-water alkalinity varies from 15.32 mM to 7.14 mM. The values are highest in the shallowest samples, with a maximum concentration of 15.32 mM at 13.45 mbsf (Fig. 18D). Concentrations then decrease to a minimum of 7.14 mM at 42.35 mbsf and increase slightly downhole to 13.40 mM at the bottom of the hole.

Downhole profiles of pore-water magnesium and calcium concentrations are very similar (Fig. 18E and 18F). The maximum concentrations are in the uppermost samples, with 46.8 mM magnesium and 9.2 mM calcium at 4.45 mbsf, below typical seawater concentrations. Between 4.45 and 13.45 mbsf, concentration of magnesium decreases to 30 mM and calcium to 5.7 mM. Pore-water concentrations of both elements are relatively constant below 13.45 mbsf, around 40 mM for magnesium and 5 mM for calcium (Fig. 18E and 18F).

Pore-water sulfate concentration is 13.78 mM at 4.45 mbsf. By 13.45 mbsf, sulfate concentrations have fallen to zero, and remain essentially zero downhole (Fig. 18G).

Ammonium concentrations increase steadily with depth, from 1.0 mM at 4.45 mbsf to 7.70 mM at 65.50 mbsf (Fig. 18H). Thereafter,

Table 7. Elemental and organic carbon compositions of sediments from Site 932.

Core, section, interval (cm)	Depth (mbsf)	IC (%)	CaCO <sub>3</sub> * (%)	TC (%)	TOC (%)	TN (%)	TS (%)	[C/N]a
155-932A-								
1H-1, 9-10	0.09	4.76	39.7	5.02	0.26	0.07	0.00	4
1H-1, 32-33	0.32	5.06	42.1	5.36	0.30	0.04	0.04	10
1H-1, 59-60	0.59	2.58	21.5	2.76	0.18	0.07	0.08	3
1H-1, 70-71	0.70	1.79	14.9	2.23	0.44	0.07	0.04	7
1H-1, 143-144	1.43	0.10	0.8	0.74	0.64	0.08	0.08	10
1H-3, 70-71	3.70	0.06	0.5	0.80	0.74	0.08	0.19	11
2H-4, 95-97	11.45	0.05	0.4	0.56	0.51	0.06	3.33	10
2H-6, 49-50	13.99	0.27	2.2	1.02	0.75	0.08	0.21	10
3H-3, 50-51	19.00	0.20	1.7	1.01	0.81	0.09	0.10	11
3H-3, 65-66	19.15	0.79	6.6	1.53	0.74	0.08	0.04	11
3H-4, 93-94	20.93	0.68	5.7	1.41	0.73	0.09	0.04	10
3H-6, 47-50	23.47	0.08	0.7	0.81	0.73	0.10	0.04	9
4H-3, 60-61	28.60	0.33	2.7	1.11	0.78	0.08	0.02	12
4H-6, 60-61	33.10	0.26	2.2	1.14	0.88	0.09	0.02	12
5H-4, 102-103	40.02	0.14	1.2	0.97	0.83	0.09	0.03	10
6H-1, 60-62	44.60	0.04	0.3	0.82	0.78	0.11	4.23	9
6H-3, 9-10	47.09	0.41	3.4	1.39	0.98	0.11	0.02	10
6H-4, 110-111	49.60	0.29	2.4	1.40	1.11	0.10	0.05	13
7H-3, 50-51	57.00	0.42	3.5	1.30	0.88	0.09	0.00	11
7H-4, 98-99	58.98	0.43	3.6	1.41	0.98	0.10	0.04	11
7H-6, 50-51	61.50	0.66	5.5	1.58	0.92	0.09	0.13	12
7H-7, 18-19	62.68	0.25	2.1	0.88	0.63	0.07	0.14	11
8H-6, 31-32	67.26	0.35	2.9	1.35	1.00	0.10	0.05	12
9H-3, 50-51	75.43	0.27	2.2	1.33	1.06	0.09	0.03	14
9H-5, 133-134	79.26	0.29	2.4	0.75	0.46	0.04	0.01	13
9H-6, 56-57	79.99	0.35	2.9	1.28	0.93	0.11	0.04	10
10H-3, 94-95	85.94	0.26	2.2	1.27	1.01	0.10	0.10	12
11X-2, 79-80	93.79	0.35	2.9	1.50	1.15	0.09	0.04	15
11X-5, 90-91	98.14	0.28	2.3	1.23	0.95	0.09	0.03	13
12X-3, 50-51	104.50	0.34	2.8	1.30	0.96	0.08	0.02	13
12X-4, 23-24	105.73	0.30	2.5	1.22	0.92	0.09	0.02	12
12X-6, 50-51	109.00	0.31	2.6	1.29	0.98	0.07	0.01	16
12X-6, 104-105	109.54	0.23	1.9	1.38	1.37	0.08	0.01	20
13X-1, 50-51	111.10	0.29	2.4	1.22	0.93	0.08	0.01	14
13X-2, 100-102	113.10	0.32	2.7	1.26	0.94	0.08	0.01	14
13X-3, 88-89	114.48	0.34	2.8	1.22	0.88	0.07	0.00	14
14X-3, 15-16	123.45	0.36	3.0	1.27	0.91	0.10	0.16	10
14X-3, 100-101	124.30	0.28	2.3	1.14	0.86	0.10	0.13	10
14X-4, 48-49	125.28	0.31	2.6	1.25	0.94	0.10	0.10	11
15X-4, 54-55	135.04	0.28	2.3	0.64	0.36	0.07	0.09	6
15X-4, 123-124	135.73	0.32	2.7	1.12	0.80	0.10	0.08	9
15X-5, 10-11	136.10	0.21	1.7	0.65	0.44	0.05	0.00	9
16X-2, 70-73	141.90	0.18	1.5	0.54	0.36	0.04	0.12	9
16X-3, 57-58	143.27	0.51	4.2	1.29	0.78	0.09	0.09	10
17X-3, 117-118	153.37	0.36	3.0	1.16	0.80	0.09	0.13	10
17X-3, 132-134	153.52	0.31	2.6	1.10	0.79	0.10	0.08	9
18X-4, 36-37	163.56	0.30	2.5	0.96	0.66	0.09	0.06	9
18X-5, 53-54	165.23	0.36	3.0	1.19	0.83	0.10	0.04	10

\*Calculated assuming all IC is calcite.

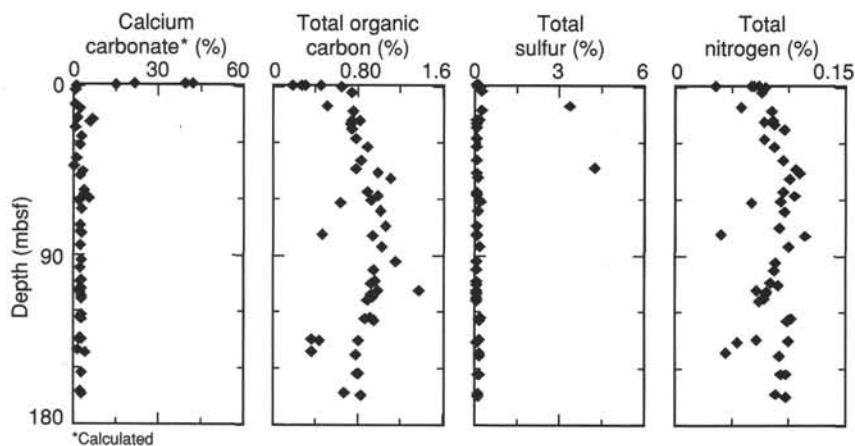


Figure 17. Concentration profiles of calcium carbonate, total organic carbon, total sulfur, and total nitrogen in Hole 932A.

the values increase more slowly to a maximum of 9.10 mM at 152.10 mbsf.

Dissolved phosphate is at a maximum in the shallowest sample, 32.7  $\mu\text{M}$  at 4.45 mbsf. The concentration drops to 9.1  $\mu\text{M}$  at 13.45 mbsf, and remains around 10  $\mu\text{M}$  downhole (Fig. 18I).

Dissolved silica concentrations range from 282 to 419  $\mu\text{M}$ . The shallowest sample has 381  $\mu\text{M}$  silica, and values then drop to be-

tween 282 and 338  $\mu\text{M}$  from 13.45 mbsf to 41.95 mbsf (Fig. 18J). Below 41.95 mbsf, the concentrations are somewhat higher and more constant, ranging from 395 to 410  $\mu\text{M}$ .

Pore-water potassium concentration is highest, 11.7 mM, in the shallowest sample (Fig. 18K). Concentrations then steadily decrease to 7.6 mM at 65.50 mbsf, potassium concentration remains relatively constant between 6.8 and 7.1 mM.

**Table 8. HI values derived from Rock-Eval pyrolysis of selected samples from Site 932.**

Core, section, interval (cm)	Depth (mbsf)	HI (mg HC/g TOC)	TOC (%)
155-932A-			
1H-1, 70-71	0.70	0*	0.44
6H-4, 110-111	49.60	55	1.11
9H-3, 50-51	74.43	40	1.06
10H-3, 94-95	85.94	37	1.01
11X-2, 79-80	93.79	31	1.15
12X-6, 104-105	109.54	29	1.15
14X-4, 48-49	125.28	22	0.94

\*Below detection limit.

Concentrations of sodium range from 463 to 471 mM, with all but one value falling between 466 and 471 mM (Fig. 18L). There is no discernible downhole trend.

Iron varies appreciably throughout the core, with concentrations between 15 and 130  $\mu\text{M}$  (Fig. 18M). The shallowest sample, at 4.45 mbsf, has a relatively high concentration of 94  $\mu\text{M}$ . Iron concentrations then drop to 25  $\mu\text{M}$  by 22.95 mbsf and reach the maximum value in the next sample at 32.45 mbsf. Thereafter, iron concentrations generally decrease, with the exception of another maximum (81  $\mu\text{M}$ ) at 97.14 mbsf.

Manganese concentrations are greatest in the shallowest sample (32.3  $\mu\text{M}$  at 4.45 mbsf; Fig. 18N). The concentration then drops to 3.9  $\mu\text{M}$  by 13.45 mbsf and remains between 2.5 and 5.0  $\mu\text{M}$  for the remainder of the core.

**Table 9. Interstitial water chemistry, Site 932.**

Core, section, interval (cm)	Depth (mbsf)	Salinity	pH	Alkalinity (mM)	Cl <sup>-</sup> (mM)	Mg <sup>2+</sup> (mM)	Ca <sup>2+</sup> (mM)	K <sup>+</sup> (mM)	HPO <sub>4</sub> <sup>2-</sup> ( $\mu\text{M}$ )	SO <sub>4</sub> <sup>2-</sup> (mM)	NH <sub>4</sub> <sup>+</sup> (mM)	H <sub>4</sub> SiO <sub>4</sub> ( $\mu\text{M}$ )	Na <sup>+</sup> (mM)	Fe <sup>2+</sup> ( $\mu\text{M}$ )	Mn <sup>2+</sup> ( $\mu\text{M}$ )
155-932A-															
1H-3, 145-150	4.45	35.5	7.39	14.36	552	46.8	9.2	11.7	32.7	13.78	1.00	381	469	94	32.3
2H-5, 145-150	13.45	33.0	7.55	15.32	554	39.0	5.7	10.4	9.1	0.13	3.10	282	467	48	3.9
3H-5, 145-150	22.95	32.0	7.55	10.23	559	39.2	5.2	10.2	8.0	0.17	4.00	292	467	25	3.5
4H-5, 145-150	32.45	32.0	7.39	7.14	560	39.6	5.3	9.9	10.4	0.01	4.90	338	463	130	3.8
5H-5, 145-150	41.95	32.5	7.56	9.79	563	38.6	5.1	9.2	9.3	0.09	5.40	295	471	85	5.0
8H-4, 145-150	65.50	32.5	7.63	9.14	563	39.4	4.8	7.6	8.6	0.23	7.70	395	469	40	3.3
11X-4, 125-135	97.14	32.0	7.74	10.59	562	40.6	4.9	7.0	11.7	0.78	8.30	395	468	81	2.7
14X-3, 140-150	124.70	32.5	7.53	13.39	562	40.0	4.6	6.8	12.1	0.15	8.60	419	471	32	2.5
17X-2, 140-150	152.10	33.0	7.79	13.40	560	40.6	5.1	7.1	11.2	0.35	9.10	410	466	15	2.5

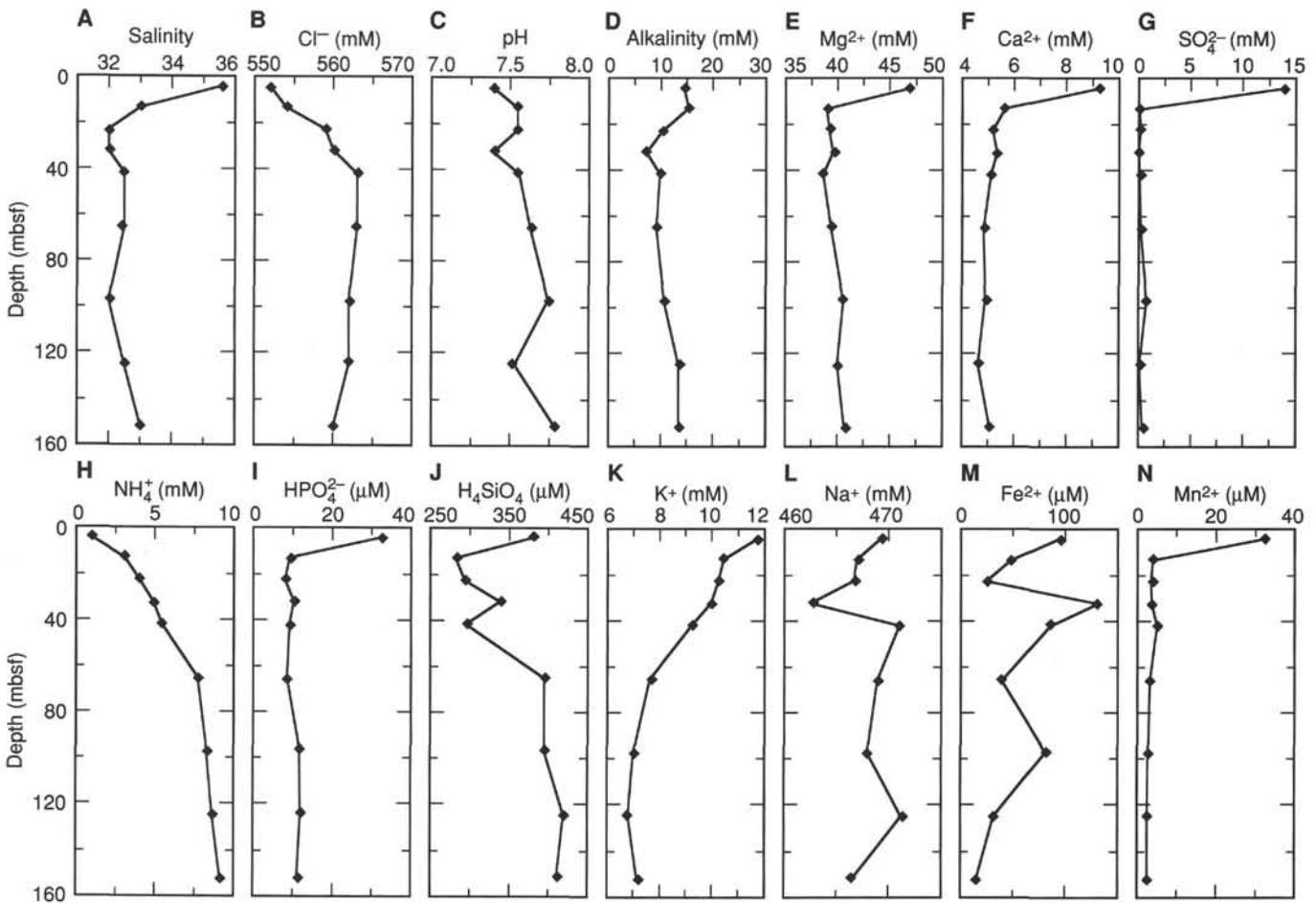


**Figure 18. Downhole variation in pore-water chemistry: A. Salinity. B. Chloride. C. pH. D. Alkalinity. E. Magnesium. F. Calcium. G. Sulfate. H. Ammonium. I. Phosphate. J. Silica. K. Potassium. L. Sodium. M. Iron. N. Manganese.**

Table 10. Major element composition (wt%) of sediment samples, Site 932.

Core, section, interval (cm)	Depth (mbsf)	Lithology	SiO <sub>2</sub>	TiO <sub>2</sub>	Al <sub>2</sub> O <sub>3</sub>	Fe <sub>2</sub> O <sub>3</sub>	MnO	MgO	CaO	Na <sub>2</sub> O	K <sub>2</sub> O	P <sub>2</sub> O <sub>5</sub>	Total	LOI
155-932A-														
8H-6, 26-30	67.21	Mud	62.53	1.12	21.76	7.95	0.13	2.11	0.80	1.25	2.99	0.21	100.82	7.97
10H-3, 89-94	85.89	Mud	61.93	1.12	21.91	7.96	0.12	2.10	0.82	1.43	2.99	0.21	100.57	8.51
11X-5, 80-85	98.04	Mud	62.14	1.11	21.90	7.99	0.12	2.15	0.84	1.48	3.00	0.21	100.92	7.93
12X-6, 99-104	109.49	Mud	61.47	1.11	21.79	7.81	0.11	2.14	0.81	1.33	2.94	0.21	99.70	8.15
13X-2, 90-94	113.00	Mud	62.97	1.11	20.85	8.06	0.12	2.07	0.92	1.44	2.86	0.20	100.60	7.59
14X-3, 95-99	124.25	Mud	63.49	1.13	20.89	7.83	0.12	2.08	0.93	1.38	2.89	0.19	100.91	7.60
15X-4, 125-30	135.75	Mud	65.07	1.07	19.69	7.11	0.10	2.02	0.99	1.41	2.78	0.19	100.41	6.81
16X-3, 58-63	143.28	Mud	63.71	1.11	20.63	7.68	0.11	2.03	0.91	1.20	2.92	0.19	100.49	7.53
17X-3, 118-124	153.38	Mud	64.61	1.09	19.39	7.23	0.11	1.93	0.93	1.47	2.77	0.18	99.70	6.89
18X-5, 55-60	165.25	Mud	63.51	1.09	20.21	7.32	0.11	1.99	0.88	1.52	2.88	0.17	99.67	7.65

Notes: Total iron is reported as Fe<sub>2</sub>O<sub>3</sub>. LOI = loss on ignition.

Table 11. Trace element composition (ppm) of sediment samples, Site 932.

Core, section, interval (cm)	Depth (mbsf)	Lithology	Ba	Ce	Cr	Cu	Nb	Ni	Rb	Sr	V	Y	Zn	Zr
155-932A-														
8H-6, 26-30	67.21	Mud	484	111	64	30	23	32	126	141	71	40	123	227
10H-3, 89-94	85.89	Mud	489	106	65	32	24	34	127	146	78	40	124	225
11X-5, 80-85	98.04	Mud	505	106	66	30	23	32	126	144	71	39	121	221
12X-6, 99-104	109.49	Mud	496	105	63	31	23	32	127	146	68	40	122	232
13X-2, 90-94	113.00	Mud	490	109	63	29	23	32	122	153	78	41	118	248
14X-3, 95-99	124.25	Mud	500	104	62	29	24	32	120	155	76	42	118	250
15X-4, 125-30	135.75	Mud	491	98	57	24	21	28	116	157	62	40	110	255
16X-3, 58-63	143.28	Mud	509	108	61	28	24	32	124	152	73	41	117	251
17X-3, 118-124	153.38	Mud	487	107	57	26	23	28	118	154	70	41	110	269
18X-5, 55-60	165.25	Mud	500	113	65	33	23	34	126	151	74	40	126	215

Overall, the pore-water profiles at this site are very similar to those observed at the previous sites. Most of the changes in pore-water chemistry occur in the upper 20 mbsf, including complete removal of sulfate. Thereafter, dissolved species such as calcium, magnesium, and alkalinity show little change. In fact, the concentrations of these three constituents below 20 mbsf (around 5 mM calcium, 40 mM magnesium, and 10 mM alkalinity) have been remarkably similar at all sites.

### Sediment Geochemistry

Ten mud samples were analyzed for major- and trace-element geochemistry (Tables 10 and 11). Samples were collected through lithologic Unit IIB, approximately every 10 m. Their geochemistry is similar to that of muds at Site 931, but shows somewhat less variability. Silica abundances are between 62 and 65 wt%; Al<sub>2</sub>O<sub>3</sub> is between

20 and 22 wt%. Abundances of Fe<sub>2</sub>O<sub>3</sub> (7.1 to 8.1 wt%) are high compared to post-Archean average shale (PAAS, 6.5 wt%), and MgO (1.9 to 2.2 wt%) is much lower (PAAS = 6.5 wt%) (Taylor and McLennan, 1985). CaO abundances are relatively constant between 0.8 and 1.0 wt%, indicating a dominant terrigenous component.

In general, SiO<sub>2</sub> increases and Al<sub>2</sub>O<sub>3</sub> decreases with depth in Unit IIB (Fig. 19). Many other elements decrease in abundance as well (e.g., Fe<sub>2</sub>O<sub>3</sub>, MgO, P<sub>2</sub>O<sub>5</sub>; Tables 10 and 11). Unit IIB is characterized by muds interbedded with silt and fine sand laminae, which increase in frequency lower in the unit. Thus, some of the observed geochemical variations likely reflect a dilution of aluminous clays by quartz-rich silt and sand.

## PHYSICAL PROPERTIES

### Index Properties

Index properties were measured for Hole 932A (Table 12). Overall, water content gradually decreases downhole from 53% just below the seafloor to 23% at the base of Hole 932A (Fig. 20). Water content decreases rapidly between the seafloor and 14 mbsf and is nearly constant between 14 and 21 mbsf. Below 21 mbsf, water content slowly decreases with depth. Between 41 and 46 mbsf, water contents are more scattered. This interval encompasses a small debris flow identified at the base of Unit IIA and the boundary between lithologic Units IIA and Unit IIB (Fig. 4). That part of the hole cored by the XCB, below 91 mbsf, is characterized by 1.5% to 3.5% decreases in water content within individual cores.

Fluctuations similar to those of water content are evident in the wet-bulk density and porosity profiles (Fig. 20). A slight decrease in bulk-density values occurs from 14 to 21 mbsf. Between 90 mbsf and the bottom of the hole, bulk density increases within individual cores. This trend is more pronounced than noted in the water content and porosity profiles (e.g., Cores 932A-11X, -12X, and -15X). These fluctuations are assumed to be an artifact of the coring process. The discrete-sample and GRAPE wet-bulk density profiles are similar but are offset. The GRAPE values are lower, and the offset progressively increases from 0.1 to 0.4 g/cm<sup>3</sup> downhole (Fig. 20). Porosity gradually decreases with depth from 75% near the seafloor to 45% at the

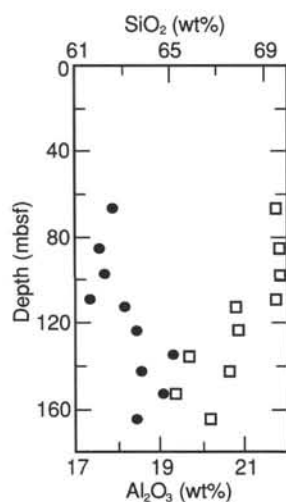


Figure 19. Depth profile of SiO<sub>2</sub> and Al<sub>2</sub>O<sub>3</sub> for mud samples. SiO<sub>2</sub> (solid circles) increases and Al<sub>2</sub>O<sub>3</sub> (open squares) decreases with depth.

Table 12. Index properties at Site 932.

Core, section, interval (cm)	Depth (mbsf)	Water content (%)	Wet-bulk density (g/cm <sup>3</sup> )	Grain density (g/cm <sup>3</sup> )	Dry-bulk density (g/cm <sup>3</sup> )	Porosity (%)	Void ratio
155-932A-							
1H-1, 29-31	0.29	49.54	1.551	2.788	0.759	72.77	2.672
1H-1, 80-82	0.80	53.38	1.498	2.780	0.677	75.65	3.107
1H-2, 79-81	2.29	52.85	1.492	2.696	0.683	74.68	2.949
1H-3, 80-82	3.80	51.01	1.516	2.719	0.723	73.43	2.763
1H-4, 80-82	5.30	47.93	1.561	2.763	0.793	71.29	2.483
2H-1, 79-81	6.79	44.83	1.577	2.779	0.867	68.79	2.204
2H-2, 79-81	8.29	43.73	1.623	2.746	0.891	67.56	2.083
2H-3, 79-81	9.79	42.60	1.669	2.718	0.915	66.32	1.969
2H-4, 78-80	11.28	41.54	1.672	2.659	0.935	64.84	1.844
2H-5, 80-82	12.80	39.31	1.723	2.734	1.002	63.35	1.729
2H-6, 79-81	14.29	40.45	1.686	2.714	0.970	64.28	1.799
3H-1, 82-84	16.32	40.56	1.661	2.763	0.973	64.79	1.840
3H-2, 77-79	17.77	40.22	1.687	2.752	0.980	64.38	1.808
3H-3, 77-79	19.27	40.49	1.679	2.752	0.973	64.64	1.828
3H-4, 82-84	20.82	40.80	1.651	2.686	0.957	64.37	1.807
3H-5, 92-94	22.42	39.62	1.623	2.731	0.994	63.63	1.749
3H-6, 103-105	24.03	38.52	1.679	2.732	1.023	62.56	1.671
3H-7, 75-77	25.25	38.89	1.720	2.761	1.017	63.17	1.715
4H-1, 74-76	25.74	36.89	1.736	2.693	1.062	60.57	1.536
4H-2, 69-71	27.19	35.87	1.699	2.726	1.096	59.81	1.488
4H-3, 87-89	28.87	36.62	1.731	2.717	1.073	60.51	1.532
4H-4, 76-78	30.26	35.83	1.769	2.768	1.103	60.13	1.508
4H-5, 94-96	31.94	34.17	1.792	2.724	1.145	57.99	1.380
4H-6, 41-43	32.91	34.31	1.794	2.755	1.146	58.42	1.405
4H-7, 67-69	34.67	35.86	1.753	2.716	1.094	59.71	1.482
5H-1, 79-81	35.29	34.43	1.789	2.763	1.144	58.61	1.416
5H-2, 79-81	36.79	34.10	1.807	2.766	1.154	58.27	1.397
5H-3, 79-81	38.29	33.41	1.804	2.753	1.172	57.41	1.398
5H-4, 80-82	39.80	34.88	1.810	2.755	1.129	59.03	1.441
5H-5, 78-80	41.28	32.11	1.833	2.760	1.214	56.03	1.274
5H-6, 78-80	42.78	34.08	1.801	2.740	1.150	58.03	1.382
5H-7, 33-35	43.83	36.63	1.758	2.774	1.081	61.02	1.565
6H-1, 100-102	45.00	32.09	1.771	2.859	1.233	56.87	1.318
6H-2, 108-110	46.58	37.48	1.773	2.588	1.029	60.22	1.514
6H-3, 91-93	47.91	33.79	1.824	2.742	1.159	57.74	1.366
6H-4, 88-90	49.38	33.27	1.803	2.703	1.167	56.81	1.315
6H-5, 87-89	50.87	32.46	1.816	2.708	1.193	55.96	1.271
6H-6, 90-92	52.40	32.67	1.831	2.762	1.197	56.68	1.308
6H-7, 73-75	53.73	33.12	1.828	2.753	1.181	57.10	1.331
7H-1, 51-53	54.01	33.62	1.785	2.707	1.158	57.24	1.339
7H-2, 42-44	55.42	33.16	1.791	2.702	1.171	56.68	1.308
7H-3, 88-90	57.38	32.59	1.824	2.751	1.197	56.49	1.298
7H-4, 79-81	58.79	32.47	1.806	2.684	1.188	55.74	1.260
7H-5, 78-80	60.28	32.04	1.808	2.691	1.202	55.32	1.238
7H-6, 63-65	61.63	32.46	1.828	2.723	1.196	56.09	1.277
7H-7, 78-80	63.28	31.96	1.832	2.768	1.220	55.93	1.269
8H-5, 50-52	66.05	31.56	1.858	2.750	1.229	55.31	1.268
8H-7, 14-16	67.54	30.07	1.880	2.741	1.275	53.49	1.150
9H-1, 42-44	72.92	31.15	1.853	2.685	1.228	54.25	1.186
9H-2, 49-51	74.25	30.56	1.858	2.707	1.252	53.76	1.163
9H-3, 90-92	75.83	29.33	1.906	2.754	1.302	52.74	1.116
9H-4, 67-69	77.10	29.59	1.874	2.719	1.285	52.73	1.115
9H-5, 44-46	78.37	28.21	1.901	2.705	1.328	50.92	1.038
9H-6, 144-146	80.87	29.17	1.894	2.773	1.311	52.71	1.115
10H-1, 37-39	82.37	31.56	1.850	2.744	1.227	55.26	1.235
10H-2, 36-38	83.86	30.97	1.836	2.705	1.238	54.23	1.185
10H-3, 65-67	85.65	29.12	1.886	2.704	1.297	52.02	1.084
10H-5, 27-29	86.74	28.28	1.919	2.713	1.327	51.08	1.044
10H-6, 74-76	88.71	28.96	1.895	2.695	1.301	51.74	1.072
10H-7, 87-89	90.34	28.77	1.920	2.765	1.323	52.15	1.090
11X-2, 83-85	93.83	31.25	1.838	2.723	1.233	54.71	1.208
11X-3, 64-66	95.14	30.51	1.854	2.716	1.255	53.80	1.164
11X-4, 62-64	96.51	30.80	1.871	2.766	1.256	54.59	1.202
11X-5, 61-63	97.85	29.52	1.893	2.737	1.292	52.81	1.119
12X-1, 41-43	101.41	30.81	1.851	2.768	1.256	54.60	1.203
12X-2, 61-63	103.11	30.28	1.878	2.722	1.264	53.58	1.154
12X-3, 64-66	104.64	28.62	1.892	2.710	1.315	51.47	1.060
12X-4, 59-61	106.09	28.36	1.902	2.734	1.330	51.37	1.056
12X-5, 62-64	107.62	27.75	1.916	2.769	1.358	50.93	1.038
12X-6, 63-65	109.13	27.01	1.938	2.765	1.383	49.97	0.999
13X-1, 79-81	111.39	30.81	1.829	2.736	1.250	54.32	1.189
13X-2, 67-69	112.77	27.88	1.895	2.729	1.345	50.73	1.029
13X-3, 66-68	114.26	28.47	1.918	2.766	1.333	51.80	1.075
13X-4, 133-135	116.38	28.44	1.891	2.728	1.325	51.41	1.058
14X-1, 97-99	121.27	29.58	1.860	2.696	1.280	52.51	1.106
14X-2, 78-80	122.58	28.75	1.899	2.774	1.326	52.21	1.092
14X-3, 76-78	124.06	27.41	1.928	2.701	1.353	49.89	0.995
14X-4, 77-79	125.57	27.62	1.919	2.696	1.345	50.11	1.004
14X-5, 116-118	127.46	28.17	1.918	2.758	1.342	51.35	1.056
15X-1, 131-133	131.31	28.77	1.901	2.747	1.319	51.99	1.083
15X-2, 73-75	132.23	27.29	1.926	2.728	1.364	49.99	1.000
15X-3, 78-80	133.78	27.98	1.915	2.724	1.340	50.81	1.033
15X-4, 78-80	135.28	26.25	1.946	2.707	1.395	48.47	0.941
15X-5, 91-93	136.91	27.58	1.974	2.766	1.364	50.70	1.028
16X-1, 41-43	140.11	28.13	1.918	2.776	1.347	51.47	1.061
16X-2, 92-94	142.12	27.22	1.912	2.710	1.362	49.73	0.989
16X-3, 91-93	143.61	26.66	1.936	2.711	1.382	49.04	0.962

Table 12 (continued).

Core, section, interval (cm)	Depth (mbsf)	Water content (%)	Wet-bulk density (g/cm <sup>3</sup> )	Grain density (g/cm <sup>3</sup> )	Dry-bulk density (g/cm <sup>3</sup> )	Porosity (%)	Void ratio
16X-4, 75-77	144.95	26.92	1.930	2.687	1.366	49.14	0.966
17X-1, 31-33	149.51	28.27	1.883	2.715	1.328	51.09	1.045
17X-2, 32-34	151.02	26.46	1.937	2.696	1.385	48.64	0.947
17X-3, 32-34	152.52	26.64	1.932	2.715	1.384	49.05	0.963
17X-4, 117-119	154.87	26.50	1.940	2.709	1.387	48.80	0.953
17X-5, 32-34	155.52	24.81	1.997	2.779	1.467	47.23	0.895
18X-1, 88-90	159.58	24.07	1.974	2.691	1.468	45.44	0.833
18X-2, 80-82	161.00	25.31	1.940	2.699	1.426	47.16	0.893
18X-3, 80-82	162.50	23.64	2.000	2.711	1.490	45.03	0.819
18X-4, 66-68	163.86	26.46	1.935	2.736	1.395	49.00	0.961
18X-5, 86-88	165.56	25.21	1.967	2.692	1.427	46.97	0.886
18X-6, 30-32	166.50	23.73	1.983	2.722	1.490	45.25	0.827

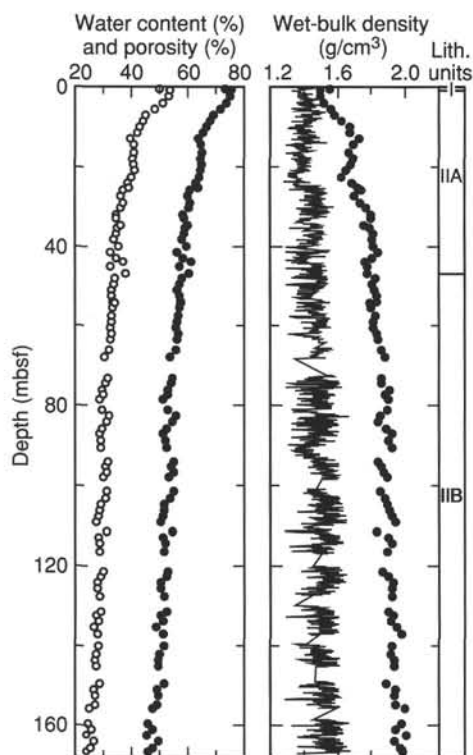


Figure 20. Water content (open symbols), porosity (solid symbols), and wet-bulk density as determined for discrete samples (circles) and by the GRAPE (line) in Hole 932A.

base of the hole. Grain density is nearly constant downhole, 2.68 to 2.78 g/cm<sup>3</sup> (Table 12).

### Compressional-wave Velocity

Pervasive microfractures produced by gas expansion restricted compressional-wave velocity measurements with the PWL to the upper 7.5 m of Holes 932A and 932B. Transverse velocities measured by the PWL range from 1470 m/s to 1960 m/s. The average in-situ velocities calculated for the 0–7.5 mbsf interval are 1497 and 1542 m/s for Holes 932A and 932B, respectively. These velocities agree well with DSV measurements from the upper 6.8 m of Hole 932A. Longitudinal velocities measured with the DSV are 1528 m/s for Unit I and 1497 to 1508 m/s for Unit IIA.

### Shear Strength

Measurements of undrained shear strength were made using the motorized shear vane on cores from Hole 932A (Table 13). The

shear-strength profile is divided into three parts: (1) seafloor to 26 mbsf; (2) 26 to 60 mbsf; and (3) 60 mbsf to the base of the hole (Fig. 21). In the first interval, undrained shear strength increases downhole from 4 kPa to 16 kPa at 26 mbsf. At 26 mbsf, shear strength increases abruptly to 22 kPa, and continues to increase to approximately 35 kPa at 60 mbsf. Measured values for this second interval are more variable than those from the upper interval. Below 60 mbsf (interval 3), values of undrained shear strength are widely scattered but increase to 80 kPa at the base of the hole (Fig. 21). The increased scatter probably results from grain-size variation, although the larger reductions in shear strength occur at core boundaries. This pattern is similar to that noted for bulk density and may be related to XCB coring disturbance.

### Resistivity

Longitudinal and transverse resistivity were determined for Hole 932A (Table 14). The longitudinal resistivity profile is divided into three segments. From the seafloor to 60 mbsf, resistivity gradually increases from 0.25  $\Omega$ m to 0.55  $\Omega$ m (Fig. 22). The resistivity of the calcareous clay of Unit I is 0.35  $\Omega$ m and approximately 0.10  $\Omega$ m higher than the resistivity of the high-water-content sediment at the top of Unit II. The resistivity anisotropy is highly variable, but generally negative in the 0–60 mbsf interval (Fig. 22). Between 60 and 140 mbsf, resistivity values are extremely uniform at about 0.4  $\Omega$ m. Sediment in this interval is essentially isotropic. Below 140 mbsf, resistivity increases downhole to approximately 0.6  $\Omega$ m at the base of the hole. The increasing scatter in this lower interval correlates with an increase in frequency of silt laminae and coarser sediment (Fig. 4). Negative and more variable anisotropy also characterizes the lower interval.

### CORE-SEISMIC INTEGRATION

Site 932 is located on the levee crest of Channel-levee System 6B (Damuth et al., 1983) and was drilled to 168.3 mbsf. Three seismic-facies units are identified using both 3.5-kHz echograms and water-gun seismic-reflection profiles obtained during Leg 155 (Figs. 2, 3, and 23). Seismic-facies Unit 1 is characterized by continuous, parallel reflections of moderate to low amplitude from 0 to 33 ms. Seismic-facies Unit 2 (33–60 ms) is acoustically transparent. Seismic-facies Unit 3 (60–350 ms), extends beyond the total drilled depth and is characterized by low-amplitude, hummocky to divergent reflections.

Preliminary correlation of lithology with acoustic units using the velocity-depth equation determined at Site 931 shows a reasonable match. However, final correlation requires more accurate determination of the velocity structure. No reflections are observed at this site that can be correlated regionally throughout the fan. However, pronounced reflections occur locally at 33 and 60 ms and mark the interfaces between the seismic-facies units.

Table 13. Undrained shear strength at Site 932.

Core, section, interval (cm)	Depth (mbsf)	Undrained shear strength (kPa)	Core, section, interval (cm)	Depth (mbsf)	Undrained shear strength (kPa)
155-932A-			8H-5, 50	66.05	36.5
1H-1, 30	0.30	7.7	8H-7, 15	67.55	28.9
1H-1, 81	0.81	7.4	9H-1, 38	72.88	41.9
1H-2, 80	2.30	3.8	9H-2, 50	74.24	58.3
1H-3, 81	3.81	6.1	9H-3, 91	75.82	44.7
1H-4, 82	5.32	6.1	9H-4, 67	77.08	28.0
2H-1, 80	6.80	9.1	9H-5, 44	78.35	30.6
2H-2, 81	8.31	7.6	10H-1, 38	82.38	20.9
2H-3, 80	9.80	7.7	10H-2, 36	83.86	42.7
2H-4, 79	11.29	9.3	10H-3, 65	85.65	50.6
2H-5, 81	12.81	10.9	10H-5, 27	86.74	32.5
2H-6, 80	14.30	10.4	11X-2, 83	93.83	21.8
3H-1, 83	16.33	10.6	11X-3, 64	95.14	32.5
3H-2, 78	17.78	9.5	11X-4, 62	96.51	38.2
3H-3, 78	19.28	13.1	11X-5, 62	97.86	39.9
3H-4, 83	20.83	12.4	12X-1, 42	101.42	20.1
3H-5, 93	22.43	9.8	12X-2, 62	103.12	34.2
3H-6, 104	24.04	12.4	12X-3, 65	104.65	33.1
3H-7, 76	25.26	13.1	12X-4, 60	106.10	43.0
4H-1, 75	25.75	16.7	12X-5, 63	107.63	46.1
4H-2, 70	27.20	21.3	12X-6, 64	109.14	41.0
4H-3, 88	28.88	22.8	13X-1, 81	111.41	19.8
4H-4, 77	30.27	24.9	13X-2, 68	112.78	37.6
4H-5, 95	31.95	22.8	13X-3, 67	114.27	46.4
4H-6, 42	32.92	17.0	13X-4, 131	116.36	19.5
4H-7, 68	34.68	22.8	14X-1, 98	121.28	27.4
5H-1, 80	35.30	22.5	14X-2, 79	122.59	39.3
5H-2, 80	36.80	21.1	14X-3, 77	124.07	43.8
5H-3, 80	38.30	20.6	14X-4, 78	125.58	54.3
5H-4, 81	39.81	19.8	15X-3, 79	133.79	45.0
5H-5, 79	41.29	28.2	15X-4, 79	135.29	58.6
5H-6, 79	42.79	21.6	15X-5, 92	136.92	65.1
5H-7, 34	43.84	20.5	16X-1, 42	140.12	29.4
6H-1, 101	45.01	33.2	16X-2, 93	142.13	34.5
6H-2, 109	46.59	25.4	16X-3, 81	143.51	45.8
6H-3, 92	47.92	35.9	16X-4, 76	144.96	37.3
6H-4, 89	49.39	41.6	17X-1, 32	149.52	30.8
6H-5, 88	50.88	26.5	17X-2, 33	151.03	41.3
6H-6, 91	52.40	25.5	17X-3, 33	152.53	53.2
6H-7, 74	53.74	25.7	17X-4, 118	154.88	54.9
7H-1, 52	54.02	26.0	17X-5, 33	155.52	67.9
7H-2, 43	55.43	26.6	18X-1, 89	159.59	67.9
7H-3, 89	57.39	30.3	18X-2, 81	161.01	46.7
7H-4, 80	58.80	34.2	18X-3, 81	162.51	65.6
7H-5, 79	60.29	28.9	18X-4, 67	163.87	56.6
7H-6, 64	61.64	24.0	18X-5, 87	165.57	71.6
7H-7, 79	63.29	30.0	18X-6, 31	166.51	80.6

Seismic-facies Unit 1 correlates with lithologic Unit I, and the upper 23 m of Subunit IIA. A prominent reflector at 33 ms apparently occurs at an increase in silt content at 25 mbsf. Seismic-facies Unit 2 correlates to the lower 21 m of Subunit IIA, which consists of silty clay with rare silt and sand laminae. Seismic-facies Unit 3 correlates with lithologic Subunit IIB. The reflector at 60 ms is near the interface between Subunits IIA and IIB.

## IN-SITU TEMPERATURE MEASUREMENTS

Temperature gradients and heat flow were determined using three downhole measurements and the bottom-water (mud-line) temperature. Two ADARA measurements were made during Cores 932A-7H (63 mbsf) and -9H (82 mbsf) using instrument number 12. The mud-line temperature reading of 2.41°C from this instrument, obtained during Core 932A-7H, was used as the reference bottom-seawater temperature at Site 932. Two successful measurements resulted in extrapolated equilibrium temperatures of 4.60°C during Core 932A-7H and 5.37°C during Core 932A-9H. One WSTP measurement was made before Core 932A-14X (120.3 mbsf) using probe thermistor number 202. This measurement provided high-quality data yielding an extrapolated equilibrium temperature of 6.01°C. We applied a correction of +462 Ω to the raw resistance values recorded by the WSTP data logger to correct for the difference in mud-line temperature recorded by the WSTP tool to that of the ADARA tool.

Equilibrium temperatures, extrapolated from synthetic curves constructed to fit transient temperature data, are plotted as a function of depth (mbsf) in Figure 24. Using the ADARA mud-line temperature, and the sub-bottom temperatures from the two ADARA and one WSTP measurements downhole, the geothermal temperature gradient can be approximated by a linear mean of 31°C/km. We calculated heat flow by adopting the constant geothermal temperature gradient of 31°C/km and a thermal conductivity,  $K$ , of  $1.2 \pm 0.15$  W/(m-K), which is an average of regression estimates to 100 mbsf. This results in a calculated heat flow of 37.2 mW/m<sup>2</sup>.

Depending on which data points are used, the geothermal gradient varies. Using the ADARA mud-line temperature and the two ADARA measurements, the geothermal gradient is 35.75°C/km (Fig. 24). If we use the two ADARA measurements and the lower temperature from the WSTP measurement (Fig. 24), the geothermal gradient is 23.37°C/km.

## SYNTHESIS AND SIGNIFICANCE

### Stratigraphic Synthesis

#### *Surficial Nannofossil-Foraminifer Clay (Unit I)*

As at Sites 930 and 931, a thin unit of brown calcareous clay (0.70 m at this site) (Fig. 25), containing foraminifers and nannofossils, overlies a brown diagenetic crust.

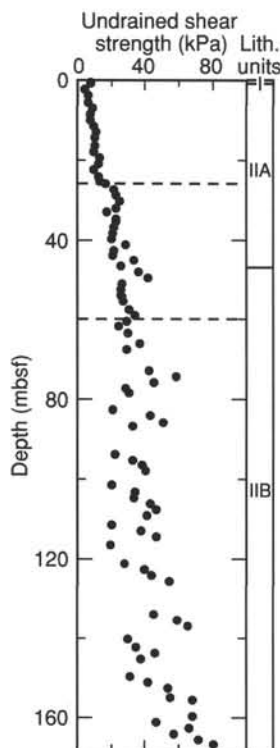


Figure 21. Undrained shear strength in Hole 932A.

#### **Bioturbated Mud Overlying Channel-levee System 6B (Subunit IIA)**

Subunit IIA (0.70–47.0 mbsf) consists of moderately bioturbated mud, passing down into mud with more abundant color banding and rare silt laminae. At 41 mbsf, a thin debris-flow deposit includes clay clasts of various shades of gray. The Lake Mungo paleomagnetic excursion (30 ka) is found at 25 mbsf and the  $Y_{p. obliq.}$  marker (40 ka) occurs at 44 mbsf. This subunit lithologically resembles Subunit IIA at Sites 930 and 931, but extends back further in time.

#### **Levee Crest of Channel-levee System 6B (Subunit IIB)**

Subunit IIB (47.0–168.3 mbsf) corresponds to the upper part of the levee crest of Channel-levee System 6B and comprises mud with thin to thick silt and fine sand beds, which increase in frequency and thickness toward the base of the subunit, particularly below 130 mbsf. These represent a fining- and thinning-upward turbidite succession.

#### **Implications**

Stratigraphic control is provided by the Lake Mungo Excursion ( $\approx 30$  ka) at 25 mbsf and the  $Y_{p. obliq.}$  marker (40 ka) at 44 mbsf. Secular variation in magnetic declination was detected with nine cycles between 31 and 44 mbsf. Estimated accumulation rates are 0.07 m/k.y. for the Holocene, 1.2 m/k.y. for the latest Pleistocene (10–30 ka) and

2.0 m/k.y. for the interval between the Lake Mungo Excursion and the  $Y_{p. obliq.}$  marker. These rates are substantially lower than at any previous sites of Leg 155 and reflect the location of Site 932 on a high-standing levee associated with the oldest channel in the Upper Levee Complex.

A palynological study at three stratigraphic levels, Holocene, last glacial (20 ka), and the  $Y_{p. obliq.}$  datum (40 ka), showed that the Holocene section is mostly barren, and greatest diversity is found in the last glacial assemblage. The pollen and spore assemblage from the 40-ka level contains lower abundances and diversities than at the 20-ka level. Evaluation of whether these changes are related to dispersal patterns or changes in vegetation in the Amazon Basin will require more shore-based study.

The sedimentological interpretations of the color-banded and turbidite sequences are similar to those discussed in detail at Sites 930 and 931. The slower sedimentation rate and greater degree of bioturbation at this site compared with Site 930 is a consequence of its position on a high-standing, older levee crest.

Although the levee crest sediment forms an overall thinning- and fining-upward succession, there is considerable lithologic variability. Some intervals have more prominent silt laminae, whereas others show more bioturbation. These data suggest considerable variation in turbidity current activity in the channel.

In general, diagenetic phenomena are similar to those observed at Sites 930 and 931. Reduced bulk density and high porosity between 14 and 21 mbsf may relate to increased sedimentation rate, diagenetic hydrotroilite formation, or the presence of a gas hydrate, but no corresponding lithologic or geochemical anomalies were detected.

#### **REFERENCES\***

- Curry, W.B., Shackleton, N.J., Richter, C., et al., in press. *Proc. ODP, Init. Repts.*, 154: College Station, TX (Ocean Drilling Program).
- Damuth, J.E., 1977. Late Quaternary sedimentation in the western equatorial Atlantic. *Geol. Soc. Am. Bull.*, 88:695–710.
- Damuth, J.E., Flood, R.D., Kowsmann, R.O., Belderson, R.H., and Gorini, M.A., 1988. Anatomy and growth pattern of Amazon deep-sea fan as revealed by long-range side-scan sonar (GLORIA) and high-resolution seismic studies. *AAPG Bull.*, 72:885–911.
- Damuth, J.E., Kowsmann, R.O., Flood, R.D., Belderson, R.H., and Gorini, M.A., 1983. Age relationships of distributary channels on Amazon deep-sea fan: implications for fan growth pattern. *Geology*, 11:470–473.
- Flood, R.D., Manley, P.L., Kowsmann, R.O., Appi, C.J., and Pirmez, C., 1991. Seismic facies and late Quaternary growth of Amazon submarine fan. In Weimer, P., and Link, M.H. (Eds.), *Seismic Facies and Sedimentary Processes of Submarine Fans and Turbidite Systems*: New York (Springer-Verlag), 415–433.
- Manley, P.L., and Flood, R.D., 1988. Cyclic sediment deposition within Amazon deep-sea fan. *AAPG Bull.*, 72:912–925.
- Taylor, S.R., and McLennan, S.M., 1985. *The Continental Crust: Its Composition and Evolution*: Oxford (Blackwell Scientific).

#### **Ms 155IR-108**

\*Abbreviations for names of organizations and publications in ODP reference lists follow the style given in *Chemical Abstracts Service Source Index* (published by American Chemical Society).

**NOTE:** For all sites drilled, core-description forms (“barrel sheets”) and core photographs can be found in Section 4, beginning on page 703. Forms containing smear-slide data can be found in Section 5, beginning on page 1199. GRAPE, index property, magnetic susceptibility, and natural gamma data are presented on CD-ROM (back pocket).

Table 14. Electrical resistivity at Site 932.

Core, section, interval (cm)	Depth (mbsf)	Longitudinal resistivity ( $\Omega$ m)	Transverse resistivity ( $\Omega$ m)	Core, section, interval (cm)	Depth (mbsf)	Longitudinal resistivity ( $\Omega$ m)	Transverse resistivity ( $\Omega$ m)
155-932A-				9H-2, 50	74.24	0.4662	0.4384
1H-1, 30	0.30	0.3523	0.3350	9H-3, 91	75.82	0.4560	0.4357
1H-1, 81	0.81	0.2732	0.2671	9H-4, 67	77.08	0.4602	0.4342
1H-2, 67	2.17	0.2599	0.2866	9H-5, 44	78.35	0.4735	0.4651
1H-2, 80	2.30	0.2544	0.2422	10H-1, 38	82.38	0.4441	0.4269
1H-3, 81	3.81	0.2516	0.2363	10H-2, 36	83.86	0.4266	0.4231
1H-4, 81	5.31	0.2562	0.2481	10H-3, 65	85.65	0.4378	0.4273
2H-1, 80	6.80	0.3310	0.2937	10H-5, 27	86.74	0.4549	0.4581
2H-2, 80	8.30	0.3424	0.3043	10H-6, 74	88.71	0.4586	0.4408
2H-3, 80	9.80	0.3446	0.3259	10H-7, 87	90.34	0.4395	0.4624
2H-4, 79	11.29	0.3269	0.3255	11X-2, 83	93.83	0.4107	0.3992
2H-5, 81	12.81	0.3995	0.3250	11X-3, 64	95.14	0.4158	0.4160
2H-6, 80	14.30	0.3832	0.3167	11X-4, 62	96.51	0.4175	0.3951
3H-1, 83	16.33	0.3771	0.3163	11X-5, 62	97.86	0.4179	0.4069
3H-2, 78	17.78	0.3760	0.3299	12X-1, 42	101.42	0.4133	0.3943
3H-3, 78	19.28	0.3600	0.3408	12X-2, 62	103.12	0.3971	0.3933
3H-4, 83	20.83	0.3692	0.3677	12X-3, 65	104.65	0.4084	0.4097
3H-5, 93	22.43	0.4266	0.3484	12X-4, 60	106.10	0.4103	0.4090
3H-6, 104	24.04	0.3607	0.3751	12X-5, 63	107.63	0.4158	0.4124
3H-7, 76	25.26	0.3753	0.3651	12X-6, 64	109.14	0.4222	0.4185
4H-1, 75	25.75	0.4287	0.3796	13X-1, 80	111.40	0.3966	0.3931
4H-2, 70	27.20	0.3844	0.3628	13X-2, 68	112.78	0.4106	0.3976
4H-3, 88	28.88	0.4444	0.3780	13X-3, 67	114.27	0.4075	0.4118
4H-4, 77	30.27	0.4040	0.3805	13X-4, 34	115.39	0.4028	0.4082
4H-5, 95	31.95	0.3994	0.4402	14X-1, 88	121.18	0.4211	0.4154
4H-6, 42	32.92	0.4128	0.4467	14X-2, 79	122.59	0.3968	0.3924
4H-7, 68	34.68	0.4524	0.4584	14X-3, 77	124.07	0.4129	0.4132
5H-1, 80	35.30	0.4613	0.3980	14X-4, 78	125.58	0.4019	0.4130
5H-2, 80	36.80	0.4241	0.4347	14X-5, 118	127.48	0.3958	0.3918
5H-3, 80	38.30	0.4676	0.3941	15X-1, 132	131.32	0.4038	0.3923
5H-4, 81	39.81	0.4118	0.4088	15X-2, 73	132.23	0.4136	0.4080
5H-5, 79	41.29	0.4914	0.5136	15X-3, 79	133.79	0.4005	0.3949
5H-6, 79	42.79	0.4496	0.4579	15X-4, 79	135.29	0.4148	0.4275
5H-7, 34	43.84	0.4481	0.4579	15X-5, 92	136.92	0.4204	0.4288
6H-1, 101	45.01	0.4711	0.4269	16X-1, 42	140.12	0.5352	0.4773
6H-2, 109	46.59	0.4705	0.4269	16X-2, 93	142.13	0.4741	0.4640
6H-3, 92	47.92	0.4820	0.4793	16X-3, 92	143.62	0.5280	0.5411
6H-4, 89	49.39	0.6700	0.4156	16X-4, 76	144.96	0.4854	0.5258
6H-5, 88	50.88	0.4548	0.4679	17X-1, 32	149.52	0.5248	0.5055
6H-6, 91	52.41	0.5030	0.4917	17X-2, 33	151.03	0.5901	0.4881
6H-7, 74	53.74	0.5201	0.5214	17X-3, 33	152.53	0.5758	0.4751
7H-1, 52	54.02	0.4744	0.4994	17X-4, 118	154.88	0.5282	0.4964
7H-2, 43	55.43	0.5611	0.4448	17X-5, 33	155.53	0.5251	0.4992
7H-3, 89	57.39	0.5155	0.4581	18X-1, 89	159.59	0.8685	0.6143
7H-4, 80	58.80	0.4979	0.4201	18X-2, 81	161.01	0.5543	0.5963
7H-5, 79	60.29	0.5173	0.4324	18X-3, 81	162.51	0.6361	0.5679
7H-6, 64	61.64	0.6804	0.4570	18X-4, 67	163.87	0.6001	0.4823
7H-7, 79	63.29	0.4708	0.4698	18X-5, 87	165.57	0.6011	0.5478
8H-5, 59	66.14	0.4554	0.4328	18X-6, 31	166.51	0.5652	0.5901
8H-7, 14	67.54	0.4690	0.4662				
9H-1, 38	72.88	0.4668	0.4340				

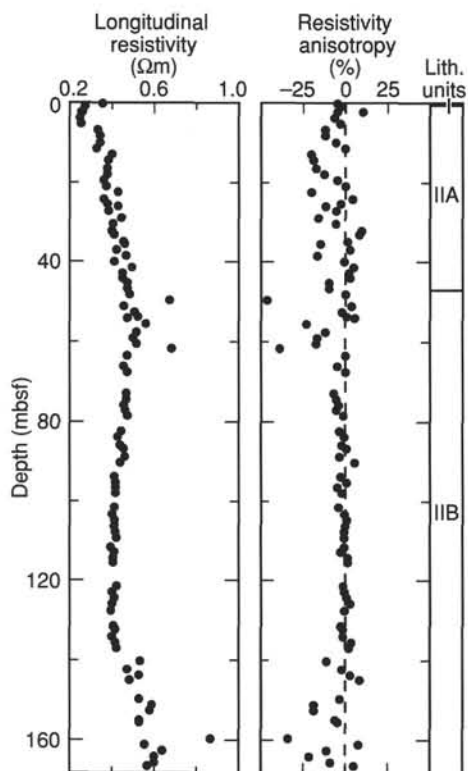


Figure 22. Longitudinal resistivity and resistivity anisotropy in Hole 932A.

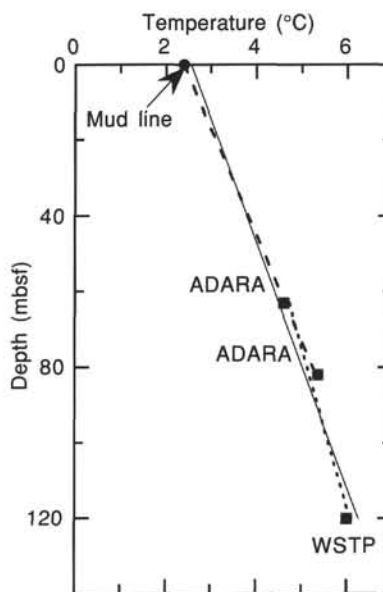


Figure 24. Estimated equilibrium temperatures in Hole 932A. A linear curve fit (solid line) through the data suggests that reliable equilibrium temperatures were acquired that indicate a geothermal gradient of 30.81°C/km. A geothermal temperature gradient of 35.75°C/km is calculated (dashed line) by using the ADARA mud-line temperature and the two ADARA measurements. A geothermal temperature gradient of 23.37°C/km is calculated (dotted line) by using the two ADARA measurements and the lower WSTP measurement.

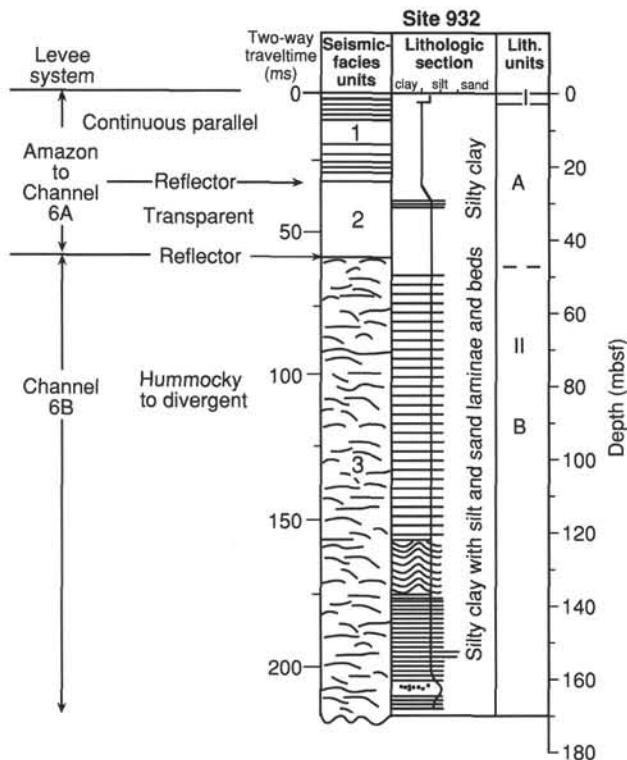


Figure 23. Correlation of lithostratigraphy with seismic-facies units and prominent reflections (arrows) on seismic profiles at Site 932.

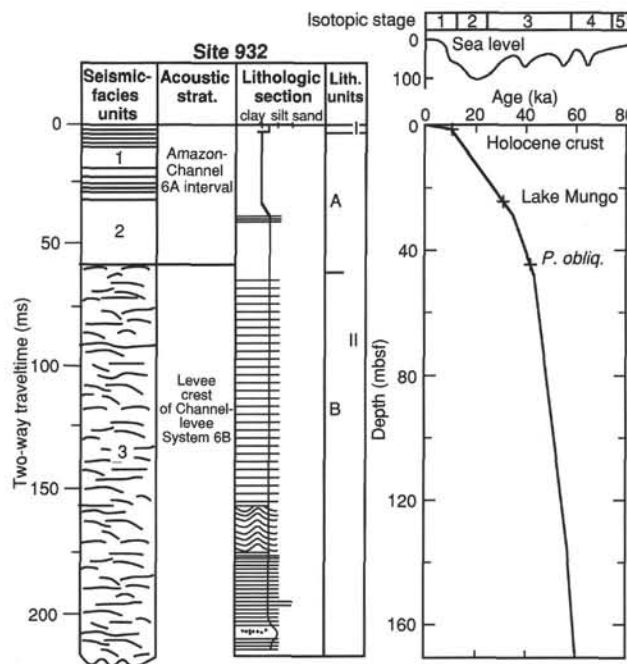


Figure 25. Summary of Site 932 showing seismic-facies units, acoustic stratigraphy, schematic lithologic column, lithologic units, chronological picks, and interpreted age-depth curve.